# STUDIES OF THE RELATIONSHIP OF PROTEIN STRUCTURE TO REGULATION AND CATALYSIS IN TYROSINE HYDROXYLASE

A Dissertation

by

GIRI RAJU SURA

Submitted to the Office of Graduate Studies of
Texas A&M University
in partial fulfillment of the requirements for the degree of

DOCTOR OF PHILOSOPHY

May 2006

Major Subject: Biochemistry

# STUDIES OF THE RELATIONSHIP OF PROTEIN STRUCTURE TO REGULATION AND CATALYSIS IN TYROSINE HYDROXYLASE

A Dissertation

by

GIRI RAJU SURA

Submitted to the Office of Graduate Studies of
Texas A&M University
in partial fulfillment of the requirements for the degree of

DOCTOR OF PHILOSOPHY

Approved by:

Chair of Committee, Paul F. Fitzpatrick
Committee Members, Gregory D. Reinhart
Michael Polymenis
J. Martin Scholtz
Head of Department, Gregory D. Reinhart

May 2006

Major Subject: Biochemistry

# ABSTRACT

Studies of the Relationship of Protein Structure to Regulation and Catalysis in Tyrosine Hydroxylase. (May 2006)

Giri Raju Sura, B.M.S., University of Health Sciences, India;

B.S., Osmania University, India;

M.S., Punjabi University, India

Chair of Advisory Committee: Dr. Paul F. Fitzpatrick

Tyrosine hydroxylase (TyrH) catalyzes the rate-limiting step in the synthesis of the catecholamine neurotransmitters dopamine, epinephrine, and norepinephrine. Phosphorylation of Ser40 of rat TyrH activates the enzyme by decreasing the affinity for catecholamines. In humans, there are four different TyrH isoforms with varying lengths for the regulatory domain. DOPA and dopamine binding studies were performed on the phosphorylated and unphosphorylated human isoforms. The $K_d$ for DOPA was increased two times upon phosphorylation of hTyrH1, but no change was seen for hTyrH4; the $K_d$ value decreased with the increase in the size of regulatory domain. The small effect on the $K_d$ value for DOPA upon phosphorylation of hTyrH suggests that DOPA does not regulate the activity of hTyrH. Dopamine binds very tightly and upon phosphorylation the affinity for dopamine is decreased. This $K_d$ value decreases with the increase in the length of the regulatory domain.

The crystal structures of substrate complexes of the homologous enzyme phenylalanine hydroxylase (PheH) show a large movement of a surface loop (residues 131-155) upon amino acid binding. The corresponding loop residues (175-200) in TyrH play an important role in DOPA formation. This conformational change in TyrH loop was studied with fluorescence anisotropy. Three tryptophan residues in the TyrH, at positions 166, 233, and 372, were mutated to phenylalanine, and Phe184 was mutated to tryptophan. An increase in anisotropy was observed in the presence of phenylalanine and 6-methyl-5-deazatetrahydropterin ($6M5DPH_4$), but the magnitude of the change of

anisotropy with 6M5DPH$_4$ was greater than that with phenylalanine. Further characterization of the sole tryptophan in the loop showed a decrease in the amplitude of the local motion only in the presence of 6M5DPH$_4$ alone.

The conformational change in wild type TyrH was examined by H/D exchange LC/MS spectroscopy in the presence of the natural ligands. Time-course dependent deuterium incorporation into the loop in the presence of ligands indicated that the pterin alone can induce the conformational change in the loop irrespective of whether iron is reduced or oxidized. From these results, one can conclude that the loop undergoes a conformational change upon pterin binding, making the active site better for amino acid binding.

# DEDICATION

This dissertation would not be possible without the loving support of so many people. I find myself overwhelmed in offering them all my thanks in dedicating this dissertation to them:

To my advisor, Dr. Paul F. Fitzpatrick, without his support this work would not have been possible.

To my mother and father, without their blessings this would not have been possible.

To my wife, Kalyani, who is my strength and purpose in life. You have gone through a very tough time and carried most of the burden so that I didn't have to. How do I say it, except: **"Thank you, my love!"**

## ACKNOWLEDGEMENTS

I would like to thank my advisor, Dr. Paul F. Fitzpatrick, for his patience and advice. I also give thanks to Dr. Colette S. Daubner for her advice and for her guidance during critical experiments. And I also give thanks to all of the lab members, past and present, who have made my graduate life enjoyable. I would like to thank Dr. Gregory D. Reinhart and Dr. Larry J. Dangott for allowing me to use equipment for my experiments. Finally, I also give thanks to my committee members for their help. And last, but certainly not least, my special thanks to the Bio/Bio staff for their administrative help.

# TABLE OF CONTENTS

Page

ABSTRACT ..... iii

DEDICATION ..... v

ACKNOWLEDGEMENTS ..... vi

TABLE OF CONTENTS ..... vii

LIST OF FIGURES ..... ix

LIST OF TABLES ..... xiii

ABBREVIATIONS ..... xiv

CHAPTER

I INTRODUCTION ..... 1

II THE EFFECTS OF PHOSPHORYLATION OF SER40 OF THE HUMAN TYROSINE HYDROXYLASE ISOFORMS ON CATECHOLAMINE BINDING ..... 13

Introduction ..... 13
Experimental procedures ..... 17
Results ..... 21
Discussion ..... 28

III MONITORING THE MOVEMENT OF THE LOOP RESIDUES 175-200 IN RAT TYROSINE HYDROXYLASE BY FLUORESCENCE ANISOTROPY ..... 32

Introduction ..... 32
Experimental procedures ..... 33
Results ..... 40
Discussion ..... 53

IV TYROSINE HYDROXYLASE DYNAMICS PROBED BY H/D EXCHANGE AND MASS SPECTROMETRY ..... 56

Introduction ..... 56

CHAPTER Page

Experimental procedures ..... 57
Results ..... 61
Discussion ..... 70

V SUMMARY ..... 73

REFERENCES ..... 74

VITA ..... 82

# LIST OF FIGURES

FIGURE Page

1 (A) Overlay of the α-C trace of the catalytic domain of human PheH (1J8U-red), rat TyrH (2TOH-green), and human TrpH (1MLW-black). The iron atom (blue) is shown to denote the active site. (B) 2-His-1-carboxylate facial triad with iron (black) of human TyrH (2TOH). .....3

2 Comparison of the active site architecture of PheH-Fe(II) in the presence and absence of bound amino acid. (A) With $BH_4$ alone (PDB-1J8U) (B) With both $BH_4$ and thienylalanine (PDB-1KW0). .....6

3 Schematic diagram of TyrH with phosphorylation sites along with protein kinases.....11

4 Catecholamine biosynthesis: Aromatic amino acid decarboxylase (AAADC), dopamine-β-hydroxylase (DBH) and phenylethanolamine -*N*-methyl transferase (PNMT). .....14

5 N-Terminal amino acid sequences of human TyrH and rat TyrH. The remaining sequence is identical among the human TyrH isoforms. The phosphorylated serine residues in rat are shown in bold.....15

6 Concentration dependence of DOPA binding to $hTyrH_1$ (filled circles) and $hTyrH_4$ (open circles). .....22

7 Spectral changes during displacement by DHN of DOPA (A) or dopamine (B and C) from unphosphorylated (A and B) and phosphorylated (C) $hTyrH_4$. Enzyme (30 μM) was incubated with 60 μM L-DOPA or dopamine for 15 min in 10% glycerol, 100 mM KCl, and 0.2 mM DTPA, 50 mM HEPES, pH 7, at 10 ºC, before the spectra indicated by solid lines were taken. DHN was then added to give a final concentration of 1 mM; the spectra indicated by dashed lines were taken after 2.8 h (A) or 12.5 h (B and C).....24

8 Effects of phosphorylation on the rate constants for association (A) and dissociation (B) of DOPA from TyrH isoforms. The conditions were as described for Figure 7 .....27

9 (A) The structures of hPheH with $BH_4$ bound (from PDB file 1J8U-green), hPheH with both $BH_4$ and thienylalanine bound (from PDB file 1KW0-yellow) and of rTyrH with 7,8-$BH_2$ bound

FIGURE Page

(from PDB file 2TOH-blue) with loops shown in pink. (B) Themovement of the 130-150 loop in PheH when an amino acid is bound. ....33

10 Sequence alignment of PheH residues (131-155) and TyrH residues (177-203) loop regions. ....33

11 Steady state kinetics of W166F/F184W/W233F/W372F rTyrH with phenylalanine as a substrate. A) tetrahydropterin oxidation; B) tyrosine formation. Conditions were as described in Experimental Procedures. The lines are from fits to the Michaelis-Menten equation. ....42

12 6-Methyl-5-deazatetrahydropterin (6M5DPH$_4$). ....42

13 Inhibition of W166F/F184W/W233F/W372F TyrH by 6M5DPH$_4$. Initial rates were determined in the presence of no (○), 50 µM (◊), 100 µM (□), 200 µM (x), or 400 µM (+) 6M5DPH$_4$. The lines are from v = (VS)/( $K$(1 + I/$K_s$) +S). Conditions: 0.5 µM W166F/F184W/W233F/W372F TyrH, 25 µM EPPS pH 7.0, 0.2 mM NADH, 2.5 µl dihydropteridine reductase (, 100 µg catalase, 10 µM $Fe(NH_4)_2SO_4$. ....43

14 Steady state fluorescence intensity of W166F/F184W/W233F/W372F rTyrH (FeIII) in 25 mM EPPS buffer, pH 7.0, at 25 ºC in the absence (○) and presence (●) of (A) 10 mM phenylalanine, (B) 500 µM 6M5DPH$_4$, or (C) both ligands. ....44

15 Steady-state fluorescence anisotropy of W166F/F184W/W233F/W372F rTyrH (FeIII) in 25 mM EPPS buffer, pH 7, at 25 ºC: (A) in the absence (empty bars) and presence (filled bars) of 10 mM phenylalanine and 500 µM 6M5DPH$_4$. (B) Change in anisotropy. ....46

16 Steady-state fluorescence anisotropy of W166F/F184W/W233F/W372F rTyrH Fe(III) in 25 mM EPPS buffer, pH 7, at 25 ºC as a function of the concentration of (A) phenylalanine (□), (B) 6M5DPH$_4$ (○), or (C) 6M5DPH$_4$ in the presence of 10 mM phenylalanine (■). ....47

17 Steady-state fluorescence anisotropy of W166F/F184W/W233F/W372F rTyrH (apo) in 25 mM EPPS buffer, pH 7, at 25 ºC: (A) in the absence (empty bars) and presence (filled bars) of 10 mM phenylalanine and 500 µM 6M5DPH$_4$. (B) Change in anisotropy. ....48

FIGURE Page

18 Comparison of the change in anisotropy of holo- and apoenzymes. Change in steady-state fluorescence anisotropy of W166F/F184W/W233F/W372F rTyrH (holo-first bar and apo-second bar) in 25 mM EPPS buffer, pH 7, with 10 mM phenylalanine and 500 μM $6M5DPH_4$.....49

19 Phase shift (open) and modulation ratio (filled) with frequency for enzyme W166F/F184W/W233F/W372F rTyrH alone (circle), with phenylalanine (diamond), with $6M5DPH_4$ (triangle) and with both (inverted triangle). The lines represent the best fit of the data to a model describing a Gaussian distribution of lifetimes.....50

20 Frequency dependence of the differential phase (open) and modulation ratio (filled) of the tryptophan fluorescence of W166F/F184W/W233F/W372F rTyrH, for enzyme alone (circle), phenylalanine (diamond), 6M5DPH4 (triangle) and both (inverted triangle). The curves represent the best fit of the data to a model describing a hindered local motion plus a global rotation (equation 9).....52

21 Isotopic patterns of deuterium atom exchanged fragments: A) EX2 mechanism and B) EX1 mechanism (*122*).....61

22 TyrH peptic peptide map. The arrows indicate the individual peptides observed from MS/MS. Loop residues are shown in bold.....64

23 Characteristics of the loop fragment in A) $H_2O$ and B) $D_2O$. The top panel is the total ion chromatograph of TyrH peptic peptides from MS-ESI, the loop fragment elution time in the middle panel and the lower panel is the enlarged region of the middle panel between 630.0 and 640.0 M/Z values.....66

24 Effects of ligands on the kinetics of deuterium incorporation into residues 174-189 in TyrH (FeIII). TyrH alone (○), 1 mM tyrosine (+), 5 mM $6M5DPH_4$ (□), and both 5 mM $6M5DPH_4$ and 1 mM tyrosine (X). The lines are fits of the data to equation 12.....68

25 Effects of ligands on the kinetics of deuterium incorporation into residues 174-189 in TyrH (FeII) upon ligand binding. TyrH alone (○), 1 mM tyrosine (+), 5 mM $6MePH_4$ (□), and both 5 mM $6MePH_4$ and 1 mM tyrosine (X). The lines are fits of the data to equation 12.....68

FIGURE Page

26 Effects of ligands on the kinetics of deuterium incorporation into residues 174-189 in TyrH (FeII) upon ligand binding. TyrH alone (○), 1 mM tyrosine (+), 1 mM $BH_4$ (□), both 1 mM $BH_4$ and 1 mM tyrosine (X), and 1mM $BH_4$, 1 mM tyrosine and equimolar NO (■). The lines are fits of the data to equation 12. .....69

# LIST OF TABLES

TABLE Page

1 Oligonucleotides Used for Construction of Expression Plasmids for Human Tyrosine Hydroxylase Isoforms. ....18

2 Steady-State Kinetic Parameters of Human Tyrosine Hydroxylase Isoforms[a] ....21

3 Kinetic Parameters for DOPA Binding to hTyrH Isoforms....26

4 Kinetic Parameters for Dopamine Binding to hTyrH Isoforms. ....28

5 Oligonucleotides Used for Construction of Expression Plasmids for Tryptophan Mutants. ....35

6 Steady State Kinetic Parameters of TyrH Tryptophan Mutants. ....41

7 Fluorescence Lifetimes of the Tryptophan in W166F/F184W/W233F/ W372F rTyrH. ....50

8 Preexponential Amplitude and Cone Angle of Tryptophan. ....52

9 Sequence of Peptic Peptides of TyrH. ....62

10 Extent of Deuterium Incorporation and Their Rates....70

## ABBREVIATIONS

| | |
|---|---|
| 6-Me$PH_4$ or 6M$PH_4$ | 6-methyl tetrahydropterin |
| 6M5D$PH_4$ | 6-methyl-5-deaza tetrahydropterin |
| $BH_4$ | tetrahydrobiopterin |
| DHPR | dihydropterin reductase |
| DOPA | dihydroxyphenylalanine |
| DTPA | diethylenetriaminepentaacetic acid |
| EDTA | ethylenediaminoetetraacetate |
| FPLC | fast protein liquid chromatography |
| HPLC | high pressure liquid chromatography |
| LC-MS | liquid chromatography - mass spectroscopy |
| NMR | nuclear magnetic resonance |
| PheH | phenylalanine hydroxylase |
| rTyrH | rat tyrosine hydroxylase |
| hTyrH | human tyrosine hydroxylase |
| TrpH | tryptophan hydroxylase |

# CHAPTER I

# INTRODUCTION

Enzymes are important biocatalysts. While the biocatalytic function lies in active site residues, the whole structure is important. The residues that are not participating in catalysis will help in aligning the active site residues and may perform additional functions such as regulation. Enzymes have evolved to use cofactors and/or redox active metal centers capable of donating a single electron to activate dioxygen. The enzymes tyrosine hydroxylase (TyrH, EC 1.14.16.2), phenylalanine hydroxylase (PheH, EC 1.14.16.1) and tryptophan hydroxylase (TrpH, EC 1.14.16.4) are pterin-dependent monooxygenases which catalyze the aromatic hydroxylation of their respective substrates (Scheme 1). The iron-dependent aromatic amino acid hydroxylases perform monooxygenase reactions utilizing tetrahydrobiopterin ($BH_4$) as the source of electrons. One atom of oxygen is incorporated into the amino acid and the other atom goes to the pterin and subsequently to form water (*1*). The eukaryotic forms of these enzymes have been studied because of their physiological importance. PheH is a liver enzyme (*2*), essential for the catabolism of phenylalanine to tyrosine. A deficiency of this enzyme causes phenylketonuria. TyrH is found in the central nervous system and the adrenal gland (*3*). The enzyme catalyzes the rate limiting step in the formation of the catecholamine neurotransmitters dopamine, epinephrine, and norepinephrine, the formation of dihydroxyphenylalanine (DOPA) from tyrosine. A deficiency of TyrH causes DOPA-responsive dystonia and Parkinson's disease (*4-6*). TrpH is also found in the brain where it catalyzes the first step in serotonin biosynthesis, the hydroxylation of tryptophan to 5-hydroxytryptophan. Decreased levels of serotonin have been implicated in depression, alcoholism, and impulsive violence (*7-9*).

---

This dissertation follows the style of *Biochemistry.*

Scheme 1

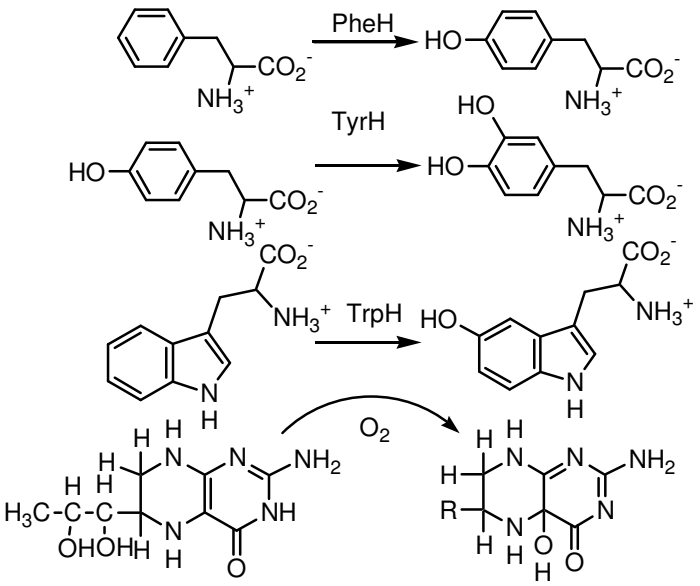


The eukaryotic amino acid hydroxylases are homotetramers (*10-12*). An equilibrium between a homodimer and a homotetramer exists only in PheH, whereas TyrH and TrpH are reported to be exclusively homotetramers (*12*). Each enzyme consists of three distinct domains: varying lengths of an N-terminal regulatory domain with little similarity among the three enzymes, a homologous C-terminal catalytic domain and a tetramerization domain. All three eukaryotic enzymes are regulated by phosphorylation of serine residues in the regulatory domain. In the case of PheH, phosphorylation activates tyrosine formation about threefold, possibly by altering the equilibrium between open and closed forms of the enzyme (*13*). In the case of TyrH, phosphorylation removes the effect of inhibition by catecholamines (*14, 15*). The role of phosphorylation has not been determined in TrpH. The crystal structures of the catalytic domains of the eukaryotic enzymes as well as of the intact PheH from *C. violaceum* have been determined (*16*). The catalytic domain structures for TyrH, PheH and TrpH with iron and pterin bound have been determined (*17-21*). A crystal structure with only amino

acid substrate bound has not yet determined. However, a structure is available for the human PheH catalytic domain with tetrahydrobiopterin and β-thienylalanine bound (*22*).

A B

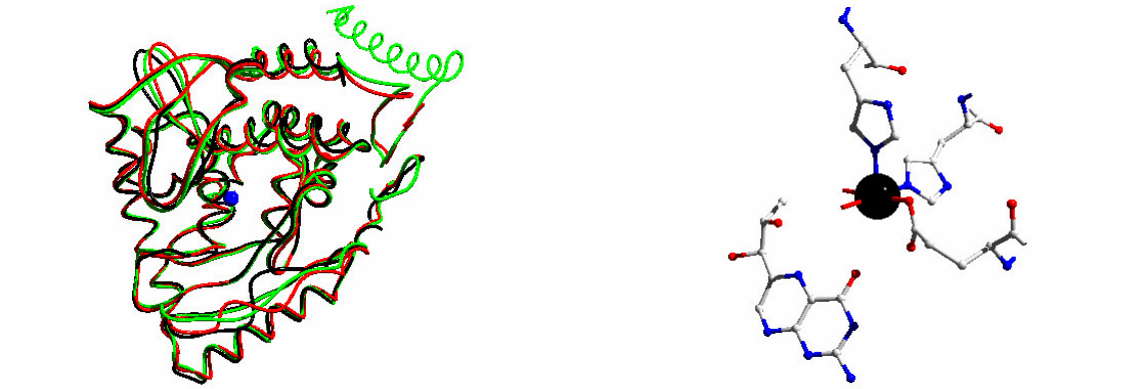

FIGURE 1. (A) Overlay of the α-C trace of the catalytic domain of human PheH (1J8U-red), rat TyrH (2TOH-green), and human TrpH (1MLW-black). The iron atom (blue) is shown to denote the active site. (B) 2-His-1-carboxylate facial triad with iron (black) of human TyrH (2TOH).

The catalytic domains of the three eukaryotic enzymes have similar structures (Figure 1A). Although the three enzymes share a homologous catalytic domain, each has a preference for its corresponding amino acid (*23-25*). PheH can hydroxylate phenylalanine and tryptophan, though tryptophan is a poorer substrate (*13*). TyrH can hydroxylate all three substrates with the preference of tyrosine>phenylalanine>tryptophan (*26, 27*). TrpH can also hydroxylate all three substrates with preferences for tryptophan≈phenylalanine>>tyrosine (*28*).

The overall structure of the catalytic domain is cup-like, with a deep active center which contains one iron atom per subunit. The iron lies at the bottom of a 10 Å deep cleft where it is bound to two histidines and one glutamate in a facial triad. In TyrH these residues are His331, His336 and Glu376 (Figure 1B); the corresponding residues in PheH are His285, His290 and Glu330. The 2-his-1-carboxylate motif is common in mononuclear, non-heme iron dependent mono and dioxygenases (*29*). In the Fe(III)

forms of the aromatic amino acid hydroxylases, the two histidine residues and the glutamate residue are joined by 3 water molecules in a distorted octahedral coordination (Figure 1B) (*17-19*). Structures of human PheH with ferrous iron have been determined both with tetrahydrobiopterin alone and with tetrahydrobiopterin and β-thienylalanine (*20, 22*). By comparing these structures, the changes in the active site upon amino acid binding to PheH can be described (Figure 2). When only $BH_4$ is bound, the iron is bound by His285, by His290, by Glu330 through monodentate coordination and by three waters (Figure 2A). In the PheH•$BH_4$•β-thienylalanine complex, glutamate 330 shifts to a bidentate coordination of the iron atom, and two of the water molecules dissociate. The iron is then five coordinate, square pyramidal, providing one open coordinate site for molecular oxygen. Differences between the binary and ternary complexes are not limited to the active site region. A loop consisting of residues 131-150 closes over the active site in the ternary complex. This movement shifts the side chain of Tyr138 about 20 Å into the active site to complete the binding site for the amino acid side chain.

According to induced-fit model (*30*), conformational changes in enzymes are necessary for substrate binding and catalysis. These conformational changes vary from domain movements to local loop movements (*31, 32*). These protein movements facilitate the binding of substrates, catalysis and release of products. For example, in human hypoxanthine guainine phosphoribosyltransferase, the crystal structure with the transition state analog immucillinGP and $Mg^{2+}$-pyrophosphate bound shows that the transition state is shielded from solvent by antiparallel β-strands. In the absence of ligands, these strands form a single random loop. This loop is proposed to recognize the substrate and shield the transition state from bulk water (*33*). Crystal structure of complexes of enzyme with substrates and transition state analogs can identify changes in structure but provide no information on the rates of which structural changes occur. A given structural change can be much faster than catalysis or rate-limiting for turnover. These structural changes span a wide range of time scales. The conformational changes that occurs on a μs to ms time scale can be identified by NMR spectroscopy (*34*) and those occurring over pico seconds to ns can be identified by fluorescence spectroscopy

(*35*), (*36*). NMR spectroscopic studies are applicable to small proteins and can give information for individual residues. In the case of triosephosphate isomerase, the solid state deuterium NMR spectrum of the protein with a single deuterium-labeled tryptophan in the loop6 hinge region reveals that the loop moves at a rate of $10^4$ $sec^{-1}$ and this matches to the turnover number (*37*). Further, studies with 5-fluorotryptophan in the loop and $^{31}$P-labelled substrate analogues using solution-state NMR spectroscopy revealed that product release is partially rate determining. T-jump relaxation spectroscopy revealed that the loop is closed only during catalysis (*37-39*). Thus in TIM a variety of approaches establish the importance of protein motions in catalysis. As a further example human cyclophillin A, a peptidy-prolyl cis/trans isomerase, catalyzes isomerization of its substrate at 9000 $s^{-1}$, and protein motions around the active site observed by NMR relaxation methods coincide with the rate of substrate rotation (*40*). Nanosecond movements around the active site in acetylcholinesterase could be observed by time-resolved fluorescence anisotropy (*36*). In recent years, several studies have been reported in which mass spectroscopy was used to use the H/D exchange behavior of water soluble proteins to probe their secondary structural changes under a wide variety of environmental conditions such as pH, temperature and ionic strength. H/D exchange rates are the rates for the amides in an entire peptide rather than for individual amides. Crystal structures of glutathione transferase suggest that the barrier for product release is a hydrogen bond between Tyr115 and Ser209. The crystal structures of the Y155F mutant did not show significant changes, but the mutant protein exhibited a 3 fold increase in activity. However, the H/D exchange mass spectroscopy of this mutant showed a 3-fold increase in exchange kinetics for the peptide at the access channel, suggesting that segmental motion in glutathione transferase is indeed responsible for the product release (*41*).

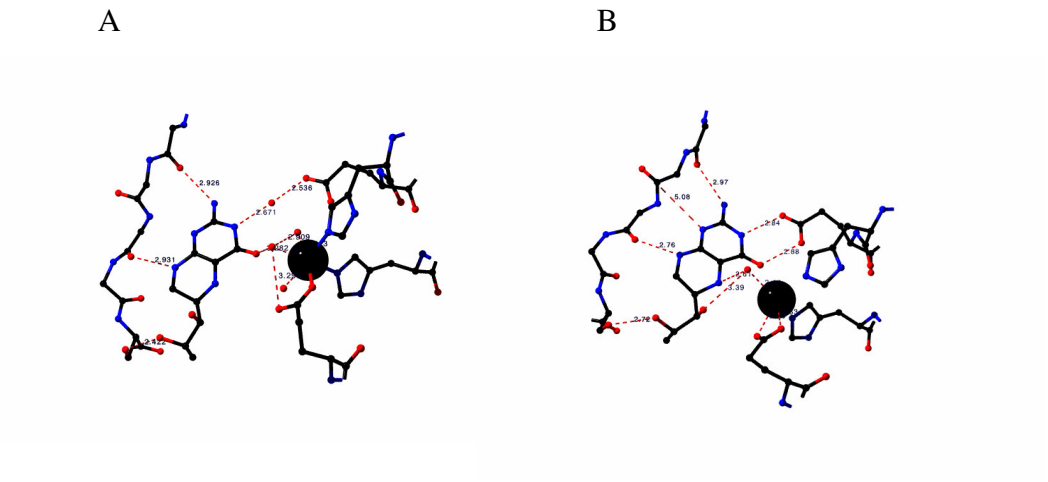


FIGURE 2. Comparison of the active site architecture of PheH-Fe(II) in the presence and absence of bound amino acid. (A) With $BH_4$ alone (PDB-1J8U) (B) With both $BH_4$ and thienylalanine (PDB-1KW0).

All members of the aromatic amino acid hydroxylase family require one atom of ferrous iron per subunit for activity (*42, 43*). Studies with rat TyrH have shown that other divalent metals will not support amino acid hydroxylation (*44*). Mutations of His285 or His290 in PheH to serine, and of His331 or His336 in TyrH to alanine abolish the activity (*45, 46*). TyrH His331E shows a decrease in affinity for iron but oxidizes tetrahydropterin in the absence of amino acid. TyrH His336Q retains hydroxylase activity but oxidation of pterin is poorly coupled to hydroxylation of amino acid (*47*). The iron atom is still required for tetrahydropterin oxidation. H336Q TyrH can utilize Co(II) to catalyze the oxidation of tetrahydropterin but not amino acid hydroxylation (*48*). The Co(II) atom would be able to form a peroxy species to promote tetrahydropterin oxidation; however, it has difficulty attaining a Co(IV) oxidation state. These results suggest that iron is strictly required to form the hydroxylating intermediate, but that other metals can support the oxidation of tetrahydropterin. In accordance with this proposal, computational studies of PheH have shown that the oxygen first interacts with the iron to form a Fe(III)-$O_2^-$ species which can then go on to form the

hydroxylating intermediate (*49*). However, this study was based on the structure of the catalytic domain of PheH with only tetrahydropterin bound. As stated above, substantial active site rearrangement occurs upon amino acid binding which may have an effect on the computational studies.

Pterin binds in a hydrophobic pocket in the active site through a stacking interaction with Phe254 in PheH or Phe300 in TyrH and numerous backbone and water-mediated hydrogen bonds (*50*). Glu332 of TyrH helps in keeping proper orientation of the pterin during catalysis (*51*) and interact with 7,8-dihydrobiopterin through a water molecule, whereas the corresponding residue Glu286 in PheH forms direct hydrogen bonds with $BH_4$. The C-4a atom of the tetrahydrobiopterin is within 4.5 Å of the open face of the iron atom, a distance which can accommodate a dioxygen molecule. In the PheH complex with β-thienylalanine and tetrahydropterin the amino acid side chain is in a hydrophobic pocket formed by Trp326, Phe331 and Pro 281 and the peptide back bone of Gly346. The amino group of Arg270 and the carboxylate group of Asp282 form electrostatic interactions with the carboxylate of the amino acid. The corresponding residue in TyrH is Arg316. Mutation of Asp328 to alanine and Arg316 to lysine greatly decreases the affinity of TyrH for tyrosine (*51*).

Until 1991, little was known about the catalytic mechanism of TyrH. Fitzpatrick showed that substrate binding is ordered with the pterin binding first, oxygen second, and finally tyrosine (*52*). A proposed chemical mechanism is shown in Scheme 2 (*53*). The mechanism can be broken down into two major steps, oxygen activation and amino acid hydroxylation. After all substrates are bound, the first step is a single electron transfer from the tetrahydropterin to oxygen to form a superoxide anion and a pterin cationic radical. This step is analogous to oxygen activation by the flavin hydroxylases and resembles the initial steps in tetrahydropterin auto-oxidation (*54*). Large $^{18}O$ isotope effects support a change in the bond order to oxygen in the first irreversible step (*55*). The same effect is found when a substrate which uncouples oxygen activation from amino acid hydroxylation is used, suggesting that oxygen activation does not involve the

amino acid substrate. Kinetic studies with alternate substrates for TyrH establish oxygen activation as rate-limiting (*27, 56, 57*).

Scheme 2

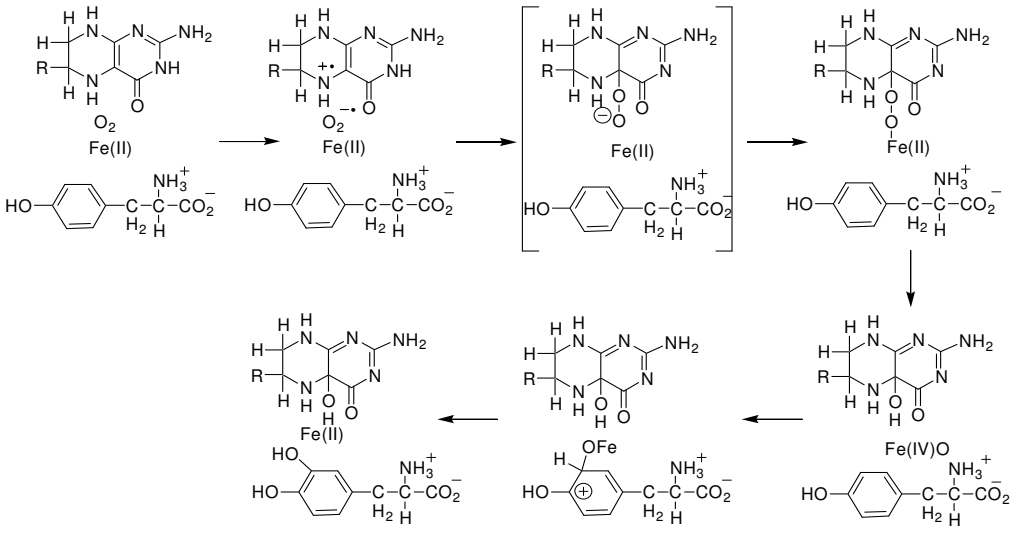


Following formation of the tetrahydropterin cation radical, the radical pair recombines to form an oxygen bridged iron-pterin species. This species undergoes heterolysis to form a high-valence, ferryl-oxo [Fe(IV)=O] species and 4a-hydroxypterin. Mutagenesis of charged active site residues has not revealed a protein based source of the required proton, suggesting that the proton is solvent derived (*51*). A deuterium solvent isotope effect of 1 is seen for wild-type TyrH, consistent with oxygen activation being the rate limiting step (*27*). In PheH, the peroxy-pterin species was proposed to be the hydroxylating intermediate in analogy to the flavin-monooxygenase family (*58*). In this case, production of the 4a-hydroxypterin and hydroxylation of the amino acid must be concerted. When serine 395 in TyrH, which is in the secondary coordination sphere of the iron, is changed to alanine, the enzyme forms 4a-hydroxypterin at a rate comparable to the wild-type enzyme but only forms DOPA at a rate 1-2% that of the wild type enzyme (*59*). This result suggests that cleavage of the O-O bond creates the hydroxylating intermediate, the proposed ferryl-oxo species. While there is no direct spectroscopic evidence for a ferryl-oxo species in the reaction catalyzed by TyrH, a

similar species has recently been characterized as an intermediate in taurine/α-ketoglutarate dioxygenase, another member of the 2-his-1-carboxylate family (*60*). The ability of the pterin-dependent monooxygenases to catalyze benzylic hydroxylation also supports the involvement of a very strong oxidant. PheH and TyrH will hydroxylate 4-methyl-phenylalanine to form 4-hydroxymethyl-phenylalanine (*56, 61*). TrpH will hydroxylate 5-methyl-tryptophan to form 5-hydroxymethyl-tryptophan (*62*). Finally, computational studies are consistent with the involvement of a Fe(IV)=O intermediate in aromatic and benzylic hydroxylation by the aromatic amino acid hydroxylases (*49*). Once formed, the proposed ferryl-oxo intermediate reacts with the aromatic ring through an electrophilic aromatic substitution mechanism, creating a cationic intermediate. Evidence for this intermediate comes from analyses of product formation using 4-X-phenylalanine substrates. The amount of product formed was proportional to the σ value for the substitute, giving a ρ value of –5 and suggesting an electron deficient transition state (*56*). This mechanism predicts an inverse secondary isotope effect on the rate of hydroxylation when ring-deuterated tyrosine is used as a substrate. In fact, when 5-$^{2}$H-tryptophan is used as a substrate for TrpH, an inverse isotope effect of 0.93 is seen (*57*). However, when 3,5-$^{2}H_2$-tyrosine is used as a substrate for TyrH, no significant isotope effect is seen (*27, 27*). This result is consistent with oxygen activation being the rate-limiting step. Following cleavage of the iron-oxygen bond, there is loss of a proton and rearomatization to form L-DOPA. The 4a-hydroxypterin dehydrates to form quinonoid dihydropterin, which tautomerizes in solution to 7,8-dihydropterin (Scheme 3) (*63*). In vivo, the quinonoid dihydropterin is reduced by dihydropterin reductase (*64*).

Scheme 3

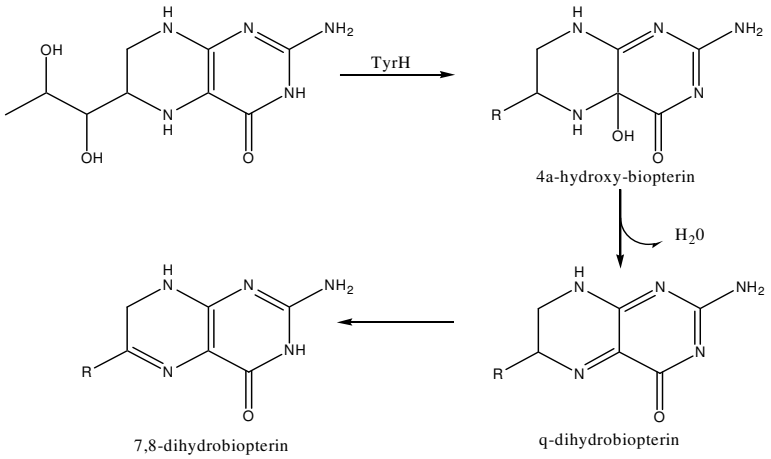


Scheme 4

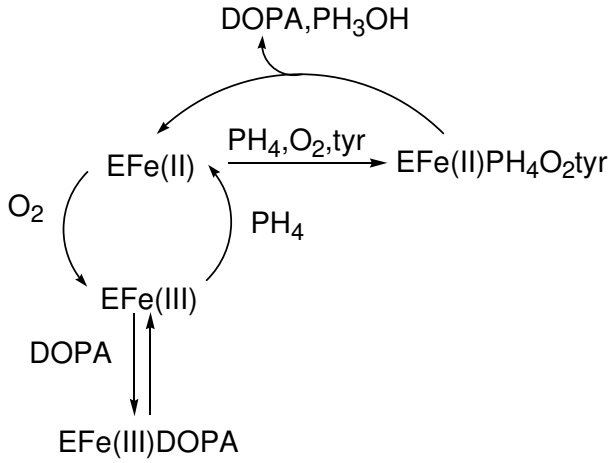


As the catalyst for the rate-limiting step in neurotransmitter production, TyrH is tightly regulated. The activity is regulated at both the transcriptional and posttranslational level (*65, 66*). Short-term regulation of catecholamine biosynthesis involves the reversible phosphorylation of serine residues in the regulatory domain of TyrH. Rat TyrH is phosphorylated at four serine residues in its amino-terminal regulatory domain by different kinases. The multisite phosphorylation of TyrH is not unique. Many proteins involved in second messenger cascades are phosphorylated by multiple kinases. Multiple phosphorylation can be required for translocation in the cell, for ubiquitination, to signal a phosphatase or an effector such as 14-3-3 protein (*67*). In

TyrH, a cdc2/cyclin kinase and extra cellular signal-regulated kinase 2 (ERK 2) ERK2 (*68*) phosphorylate Ser8 (*69, 70*). Ser19 is phosphorylated by p38 regulated/activated kinase (*71*). Both Ser19 and Ser40 are phosphorylated by calmodulin-dependent protein kinase with more preference for Ser19 (*72*) and by mitogen-activated protein kinase 2 (MAPKAP 2) with more preference for Ser40 (*73*). The target of cyclic dependent kinase 5 (Cdk5) and ERK2 (*68*) is Ser31. Cyclic AMP-dependent protein kinase (PKA) (*72*), protein kinase C (*74*), mitogen-activated protein kinase-activated protein kinase1 (MAPKAP kinase 1) (*73*), mitogen and stress-activated protein kinase 1 (*71*), and cGMP-Dependent protein kinase (*75*) all catalyze the phosphorylation of Ser40 (Figure 3).

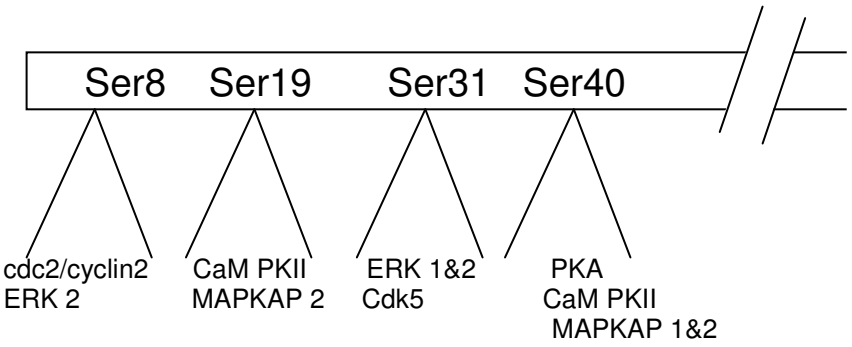


FIGURE 3. Schematic diagram of TyrH with phosphorylation sites along with protein kinases.

TyrH is regulated by feedback inhibition due to its product DOPA binding to the ferric iron (Scheme 4). In TyrH, Daubner et al. reported that activation of tyrosine hydroxylase by phosphorylation of Ser40 is due to alleviation of inhibition by catecholamines (*15, 76*). Phosphorylation of Ser40 in TyrH results in a 17-fold decrease in affinity for DOPA and in a 300-fold decrease in the affinity for dopamine. A structural change between residues 33-50 in the regulatory domain upon phosphorylation at Ser40 makes the region trypsin sensitive whereas dopamine bindig does not (*77*). The phosphorylation of serines by different kinases under different conditions with different specificities has complicated the understanding of the TyrH activity. Mutational studies

of serines to glutamate to mimic isosteric serine-phosphorylation and to alanine to mimic unphosphorylation have been carried out. A negative charge at Ser8, Ser19 and Ser31 does not significantly affect the binding of DOPA and dopamine, but does increase the thermal stability (*78*). To restore catalytic activity the ferric iron must subsequently be reduced. Tetrahydropterins are capable of reducing the iron, and they are proposed to be the reductant *in vivo* due to their role as substrate for the enzyme (*79, 80*).

The situation in human TyrH is somewhat complicated because of four different isoforms. These isoforms are formed due to differential splicing of mRNA. hTyrH isoform 1 corresponds to rat enzyme, hTyrH2 contains four amino acid residues after Met30, hTyrH3 contains 27 residues inserted after Met30, and hTyrH4 contains 31 amino acid residues consisting of the insert in hTyrH2 followed by that in hTyrH3.

The combined data from mutational and spectroscopic studies have resulted in an understanding of the mechanism of regulation in human isoforms and protein dynamics upon ligand binding. This dissertation will describe experiments and results which report on the regulatory role of the human isoforms and on the loop movement in the catalytic domain upon ligand binding.

# CHAPTER II

## THE EFFECTS OF PHOSPHORYLATION OF SER40 OF THE HUMAN TYROSINE HYDROXYLASE ISOFORMS ON CATECHOLAMINE BINDING*

### INTRODUCTION

The biosynthesis of the catecholamine neurotransmitters begins with the hydroxylation of tyrosine to form dihydroxyphenylalanine (DOPA) (Figure 4). This step, catalyzed by the enzyme tyrosine hydroxylase (TyrH), is generally accepted to be the rate-limiting step in the pathway (*81*). The TyrH reaction is a monooxygenation, in that molecular oxygen is the source of the atom of oxygen incorporated into DOPA (*82*), while tetrahydrobiopterin serves as the source of the two electrons required for reduction of the other atom of oxygen to the level of water. Activation of oxygen for the reaction involves an active site nonheme iron atom; for catalysis, the iron atom must be in the ferrous form (*44*). In the presence of oxygen the iron is readily oxidized to the ferric form; tetrahydropterins can reduce the iron back to the active ferrous state (*79*). The active site containing this iron atom is a deep cleft in a catalytic domain of about 300 amino acids that is homologous to the catalytic domains of the two other pterin-dependent aromatic amino acid hydroxylases, phenylalanine hydroxylase and tryptophan hydroxylase (*17, 83*).

---

*Reproduced with permission from "Effects of Phosphorylation by Protein Kinase A on Binding of Catecholamines to the Human Tyrosine Hydroxylase Isoforms" by Sura, G.R., Daubner, S.C. and Fitzpatrick, P.F, 2004, *J. Neurochem.* 90, 970-980, Copyright 2004 by Blackwell (*84*).

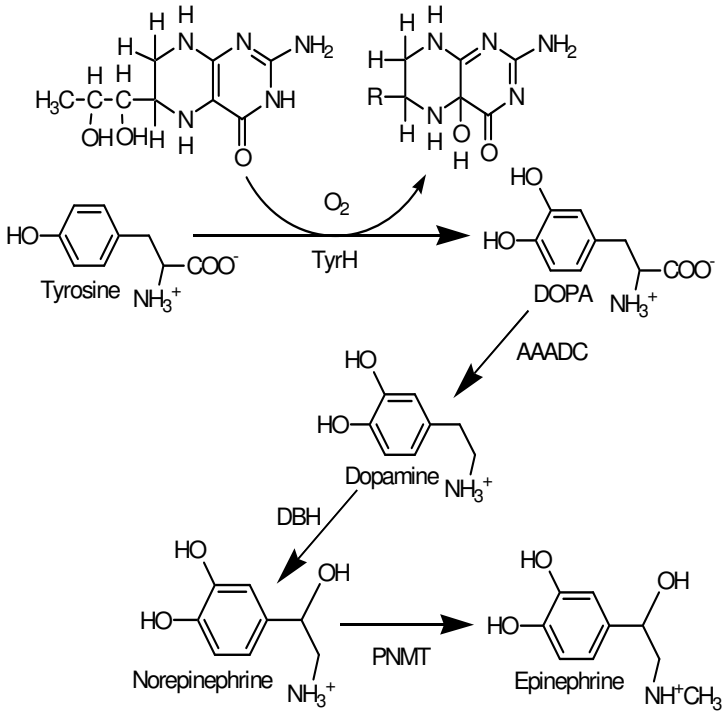


FIGURE 4. Catecholamine biosynthesis: Aromatic amino acid decarboxylase (AAADC), dopamine-β-hydroxylase (DBH) and phenylethanolamine-*N*-methyl transferase (PNMT).

In humans, tissue-specific expression of four different TyrH isozymes has been reported (*85*). This protein diversity is generated through alternative splicing of the pre-mRNA from the single TyrH gene (*85*). The differences among the isozymes are all limited to the regulatory domain (Figure 5). Isoform 1 most closely resembles rat TyrH. Isoform 2 contains an additional 4 amino acids between amino acids 30 and 31 of isoform 1, isoform 3 contains an insertion of 27 amino acids at the same point and isoform 4 contains both insertions, giving 31 additional residues at the same position. All four isoforms have been found in human brain (*86*). Isoforms 1, 2 and 4 have been reported in human adrenal medulla, whereas isoform 1 and 2 are predominant in the locus coeruleus and substantia nigra of brain (*85*). Each human TyrH isoform has a serine homologous to Ser40 of rat TyrH, the serine modified by cAMP-dependent

protein kinase A (PKA). In the human isozymes these serines are numbered 40, 44, 67 and 71 (Figure 5).

```
rTyrH  MATPSAPSPQPKGFRRAVSEQDAKQAEAVT--------------------------------SPRFIGRRQS 40
hTyrH1 MATPDATTPQAKGFRRAVSELDAKQAEAIM--------------------------------SPRFIGRRQS 40
hTyrH2 MATPDATTPQAKGFRRAVSELDAKQAEAIMVRGQ----------------------------SPRFIGRRQS 44
hTyrH3 MATPDATTPQAKGFRRAVSELDAKQAEAIM----GAPGPSLTGSPWPGTAAPAASYTPTPRSPRFIGRRQS 67
hTyrH4 MATPDATTPQAKGFRRAVSELDAKQAEAIMVRGQGAPGPSLTGSPWPGTAAPAASYTPTPRSPRFIGRRQS 71
```

FIGURE 5. N-Terminal amino acid sequences of human TyrH and rat TyrH. The remaining sequence is identical among the human TyrH isoforms. The phosphorylated serine residues in rat are shown in bold.

All three enzymes also contain N-terminal regulatory domains. The sequences of these regulatory domains differ among the three enzymes, consistent with their discrete regulatory properties. In the case of TyrH, short term increases in the formation of DOPA in vivo correlate with increased phosphorylation of serine residues in this regulatory domain (*65, 87*). In rat TyrH, the serine residues which exhibit altered phosphorylation when dopamine biosynthesis is stimulated are located at positions 19, 31, and 40; Ser8 has also been found to be phosphorylated in adrenal cells, but no physiologically relevant conditions which alter its level of phosphorylation have been described (*87*). A large number of studies have examined the effects of such phosphorylation on the catalytic activity of TyrH in vitro, utilizing protein kinases specific for selected sites (*65, 66, 81*). cAMP-Dependent protein kinase A (PKA) was demonstrated early on to be specific for Ser40 (*72*), and more recently the MAP kinases ERK1 and ERK2 have been demonstrated to phosphorylate Ser31 (*88, 89*). No kinase specific for Ser19 has been described to date, but several will phosphorylate both Ser19 and Ser40 (*72, 73*). Activation of TyrH upon phosphorylation by PKA has been demonstrated by a number of laboratories (*65, 66, 81*). However, the effects on the enzyme activity are quite modest, changes of about two-fold in the $K_m$ value for tetrahydrobiopterin (*76, 90*) and the $K_i$ value for dopamine (*90*), when purified recombinant enzyme is used. The degree of activation upon phosphorylation by a MAP kinase is smaller (*73, 88*), while phosphorylation of both Ser19 and Ser40 has a

comparable effect to phosphorylation of Ser40 alone (*73*). In the case of rat TyrH, Ser40 phosphorylation results in much more dramatic effects on the affinity of the ferric enzyme for catecholamines due to modest increases in the rate constants for binding of catecholamines and much larger increases in the rate constants for dissociation (*15, 91*). The greatest effects are seen upon binding of dopamine, norepinephrine, and epinephrine; the rate constants for dissociation of all three increase by three orders of magnitude when Ser40 is phosphorylated, while the dissociation rate constants for DOPA increase about 20-fold. These results are consistent with the model of Scheme 4 for the effects of Ser40 phosphorylation on rat TyrH (*15, 76*). The active ferrous form of the enzyme catalyzes the formation of DOPA from tyrosine. This form of the enzyme can be oxidized to the inactive ferric form; reduction by tetrahydrobiopterin restores activity. However, if a catecholamine accumulates in the cell, it can bind to the ferric enzyme, trapping it in the inactive complex. Consistent with such a model, when TyrH is isolated from rat or bovine cells, it is in the form of a complex containing ferric iron and bound catecholamines (*92, 93*). The rate constants for dissociation of dopamine, norepinephrine, and epinephrine from the rat enzyme suggest that catecholamine binding to the ferric enzyme is effectively irreversible in the cell until Ser40 is phosphorylated (*91*).

In humans four different TyrH isoforms are synthesized from this single gene by differential splicing (*85, 94, 95*). Characterization of recombinant forms of all four human isoforms has shown that their steady state kinetic parameters are not dramatically different (*43, 90, 96*), although $hTyrH_1$ is reported to have a slightly higher $K_m$ for tetrahydrobiopterin (*90*). The effects of phosphorylation by different kinases on steady state kinetic parameters are reported to be comparable for all four isoforms (*73*), although there is one report that $hTyrH_3$ is not activated significantly upon phosphorylation by PKA (*97*). However, as noted above the primary effect of phosphorylation on the rat enzyme is not on the steady state kinetic parameters but on the binding of inhibitory catecholamines. The goals of the experiments described here were to determine if the mechanism of Scheme 4 was equally applicable to human and

rat TyrH and whether the different human isoforms differ in the effect of phosphorylation of Ser40 on the binding of DOPA and dopamine.

## EXPERIMENTAL PROCEDURES

*Materials*. L-Tyrosine was purchased from Sigma Chemical Corp., St Louis, MO. 6-Methyltetrahydropterin ($6MPH_4$) was purchased from B. Schircks Laboratories. All other reagents were of the highest purity commercially available. The catalytic subunit of beef heart PKA was purifed by the method of Flockhart and Corbin (*98*).

*Construction of vectors for expression of human tyrosine hydroxylase isoforms in E. coli.* Plasmid pHTh-63, which contains the cDNA for $hTyrH_2$, was a gift from Dr. Karen O' Malley, Washington University, St. Louis. PCR was used to add an *Nco*I site at the 5' end of the coding region and a *BamH*I site at the 3' end, allowing insertion into the pET-23d expression vector (Novagen). Plasmids containing $hTyrH_2$ cDNA were identified by restriction enzyme digestion and confirmed by sequencing; the plasmid selected for further use was named p23dHTH2. To obtain the other human isoforms, modifications of the QuikChange method (Stratagene) were used to delete or insert DNA coding for multiple amino acids. To obtain p23dHTH4, the plasmid for expression of $hTyrH_4$, two separate PCR reactions, each containing only one of the oligonucleotides in Table 1, were run for five cycles. The two reactions were then combined for twelve additional PCR cycles. To obtain the plasmids for expression of $hTyrH_1$ and $hTyrH_3$, p23dHTH1 and p23dHTH3, respectively, the oligonucleotides in Table 1 were used to delete 12 base pairs after the codon for Met30, using p23dHTH2 and p23dHTH4 as templates. To avoid formation of dimers between the primers, only one oligonucleotide primer was present for the first PCR cycle, and the other was then added for the remaining 17 cycles. The desired plasmids were identified by restriction digestion and confirmed by sequencing.

**Table 1. Oligonucleotides Used for Construction of Expression Plasmids for Human Tyrosine Hydroxylase Isoforms.**

| Modification | Product | Plus strand oligonucleotide | Minus strand oligonucleotide |
|---|---|---|---|
| Deletion of 12 base pairs from p23dHTH2 | p23dHTH1 | 5'-GGCAGAGGCCAT CATGTCCCCGCGGT TATTGGG-3' | 5'-CCCAATGAACCG CGGGGACATGATGG CCTCTGC-3' |
| Insertion of 81 base pairs into p23dHTH2 | p23dHTH4 | 5'-CCGTGGCCTGGAA CTGCAGCCCCAGCT GCATCCTACACCCC CACCCCAAGGTCCC CGCGGTTCATTGGG CG-3' | 5'-GCAGTTCCAGGC CACGGAGAGCCTGT GAGGCTGGGCCCCG GGGCGCCCTGCCCTT TACCATGATGGCTCT GC-3' |
| Deletion of 12 base pairs from p23dHTH4 | p23dHTH3 | 5'-GCAGGCAGAGGC CATCATGGGCGCCC CGGGGCCCAGCCTC ACAG -3' | 5'-GCTGGGCCCCG GGGCGCCCATGATG GCCTCTGCCTGCTTG GC -3' |

*Purification*. Expression and purification of the human enzymes was performed using modifications of methods developed for the rat enzyme (*76*). *E. coli* BL21 Star™ (DE3) cells transformed with p23dHTH1, p23dHTH2, p23dHTH3 or p23dHTH4 were grown in Luria Bertani medium containing 100 μg/ml carbenicillin at 25˚C. When the absorbance at 600 nm reached 0.5, expression was induced with 0.5 mM isopropyl-ß-D-thiogalactopyranoside. After 6 hours, cells were harvested by centrifugation and resuspended in 75 μM diethylenetriaminepentaacetic acid (DTPA), 10% glycerol, 1 μM pepstatin, 1 μM leupeptin, 100 μg/ml phenylmethylsulfonylflouride, 25 μg/ml lysozyme, 50 mM HEPES, pH 7.0. The cells were lysed by sonication at 4 ˚C and centrifuged at 28,000 x g for 30 min. Streptomycin sulfate was added to the supernatant to a final concentration of 1% to allow precipitation of nucleic acids at 28,000 x g for 20 min. The resulting supernatant was made 45% saturated in ammonium sulfate, stirred for 20 min and centrifuged for another 20 min. The resulting pellet was resuspended in 75 μM DTPA, 10% glycerol, 50 mM HEPES, pH 7.0, and dialyzed against the same buffer. After centrifugation to remove precipitated protein, the sample was loaded onto a Hitrap-

Heparin column; this was eluted with a linear gradient of 0-0.8 M KCl in 75 μM DTPA, 10% glycerol, 50 mM HEPES, pH 7.0. Fractions containing tyrosine hydroxylase were pooled and precipitated by making the solution 65% saturated in ammonium sulfate. The pellet was resuspended to give a concentration of ~300 μM TyrH in 100 mM KCl, 10% glycerol, 1 μM pepstatin, 1 μM leupeptin, 50 mM HEPES, pH 7.0. To this, ferrous ammonium sulfate was added to give a 20% molar excess of iron over TyrH active sites; excess iron was removed by dialysis (*91*). All protein purification steps were carried out at 4 ºC. Purified enzymes were stored at -80 ˚C. Typical yields were 150-200 mg of pure protein from 6 L of culture.

*Assays*. The iron contents of the purified enzymes were determined by atomic absorption spectrophotometry as previously described for the rat enzyme (*79*). Concentrations of the purified proteins were determined using an $A_{280}^{1\%}$ value of 10.4 (*92*). A colorimetric end point assay for DOPA was used to measure tyrosine hydroxylase activity (*52*). Assays were carried out in 100 μg/ml catalase, 1 mM dithiothreitol, 10 μM ferrous ammonium sulfate, at 32 ºC. Standard conditions include 0.5 μM enzyme, 400 μM $6MPH_4$ and 200 μM tyrosine in 50 mM HEPES, pH 7.0. For determination of the $K_m$ value for tyrosine, assays contained 400 μM $6MPH_4$ and 10 to 360 μM tyrosine. For determination of the $K_m$ value for $6MPH_4$, assays contained 200 μM tyrosine and 10 to 360 μM $6MPH_4$. 6-Methyltetrahydropterin was used as substrate because the substrate inhibition seen with tyrosine in this case is much less than when tetrahydrobiopterin is used, allowing intrinsic kinetic parameters to be more readily measured (*52*). To obtain the kinetic parameters in Table 2, the kinetic data were fit to the Michaelis-Menten equation using the program KaleidaGraph (Synergy Software).

*Phosphorylation of tyrosine hydroxylase*. The method for phosphorylation of human tyrosine hydroxylase was based on that developed for the rat enzyme (*15*). Each TyrH isoform (20 μM) was incubated with 60 μM ATP, 6 mM $MgCl_2$, and 100 nM PKA catalytic subunit in 100 mM KCl, 10% glycerol, 50 mM HEPES, pH 7.0, at 4 ˚C. After 2 hours, additional ATP, $MgCl_2$ and PKA were added to yield final concentrations of 125 μM, 12.5 mM, and 200 nM, respectively; the reaction was continued for 6 hours. The

phosphorylated enzyme was isolated on a MonoQ column using a gradient of 0-500 mM NaCl in the same buffer. The phosphorylation status was confirmed by incubating a sample of phosphorylated enzyme eluted from the MonoQ column with 15 mM $MgCl_2$, 88 nM PKA, 560 μM [$\gamma$-$^{32}$P]ATP ($1.97x10^5$ cpm/nmol) in 10% glycerol, 50 mM HEPES, pH 7.0, at room temperature. Aliquots were removed at five minute intervals for 15 minutes and spotted onto phosphocellulose filter paper; these were washed twice with 75 mM phosphoric acid and once with acetone. The amount of radioactivity remaining on the filters was determined by scintillation counting. In all cases the previously phosphorylated enzymes incorporated less than 0.02 nmol phosphate/nmol TyrH; unphosphorylated enzyme incorporated a stoichiometric amount of phosphate under these conditions.

*Catecholamine binding*. Catecholamine binding studies were performed by using previously described procedures (*15*). To determine the rate constants for dissociation of DOPA and dopamine, 40 μM unphosphorylated or phosphorylated TyrH was incubated with 60 μM DOPA or dopamine in 100 mM KCl, 10% glycerol, 50 mM HEPES, pH 7.0, at 10 ˚C. Formation of the enzyme-catecholamine complex was monitored by observing the increase in absorbance at 690 nm (*43*). After formation of the catecholamine complex was complete, 2,3-dihydroxynaphthalene (DHN) was added to give a final concentration of 1 mM; the increase in absorbance at 550 nm due to formation of the enzyme-DHN complex was then monitored. The dissociation rate constant was calculated by fitting the absorbance versus time to equation 1.

$$A_t=A_\infty+ (A_0-A_\infty)\, e^{-kt} \qquad (1)$$

To determine association rate constants, 125 μM - 2 mM DOPA or dopamine was mixed with 15 μM (final concentrations) tyrosine hydroxylase in an Applied Photophysics SX-18MV stopped flow spectrophotometer. The increase in absorbance at 690 nm was monitored and the resulting data fit to equation 1.

**RESULTS**

*Characterization of human tyrosine hydroxylase isoforms.* Plasmids were constructed for expression of all four human TyrH isoforms in *E. coli* by starting with the cDNA for $hTyrH_2$. All four proteins expressed well and could be purified using the protocol developed for the rat enzyme. The specific activities of the purified hTyrH isoforms were comparable: 1.8 $\mu mol\text{-}min^{-1}\text{-}mg^{-1}$ ($hTyrH_1$), 1.2 $\mu mol\text{-}min^{-1}\text{-}mg^{-1}$ ($hTyrH_2$), 1.3 $\mu mol\text{-}min^{-1}\text{-}mg^{-1}$ ($hTyrH_3$) and 1.5 $\mu mol\text{-}min^{-1}\text{-}mg^{-1}$ ($hTyrH_4$). After incubation with a slight excess of ferrous ammonium sulfate and removal of excess iron, each isoform contained one atom of iron per monomer. The steady state kinetic parameters with tyrosine and $6MPH_4$ as substrates were measured for each isoform and are summarized in Table 2. The $V_{max}$ and $K_{tyr}$ values are essentially the same among all four isoforms. The $K_m$ values for $6MPH_4$ for isoforms 2-4 are similar, while that for $hTyrH_1$ is slightly larger.

**Table 2. Steady-State Kinetic Parameters of Human Tyrosine Hydroxylase Isoforms[a].**

| Enzyme | $K_{tyr}$ (μM)[b] | $K_{6MPH4}$ (μM)[c] | $V_{max}$ ($min^{-1}$) |
|---|---|---|---|
| **$hTyrH_1$** | 77 ± 10 | 116 ± 10 | 135 ± 7 |
| **$hTyrH_2$** | 66 ± 5 | 75 ± 6 | 100 ± 2 |
| **$hTyrH_3$** | 79 ± 9 | 70 ± 9 | 119 ± 5 |
| **$hTyrH_4$** | 73 ± 6 | 63 ± 5 | 108 ± 3 |

[a]Conditions: 100 μg/ml catalase, 1 mM dithiothreitol, 10 μM ferrous ammonium sulfate, 50 mM HEPES, pH 7.0, 32 ºC. [b]400 μM $6MPH_4$. [c]200 μM tyrosine.

*Catecholamine binding.* Previous analyses of rat TyrH have shown that phosphorylation has a large effect on the binding of catecholamines to the ferric form of the enzyme (*15*). The rate constants for dissociation and association of DOPA and dopamine were determined for all four human isoforms by monitoring the formation of the broad charge-transfer absorbance band centered at 690 nm due to the complex. In the

case of complex formation, the rate constants were determined by mixing the enzyme with various concentrations of DOPA or dopamine (data not shown). The observed rate constants for binding derived from these analyses show a linear dependence on the concentration of DOPA or dopamine, as illustrated in Figure 6 for DOPA binding to unphosphorylated $hTyrH_1$ and $hTyrH_4$. This behavior is consistent with a simple bimolecular binding reaction. The second order rate constants for binding of DOPA or dopamine to each of the isoforms could be determined from the slopes of plots such as those in Figure 6. The resulting values are summarized in Tables 3 and 4. The values decrease slightly as one proceeds from isoform 1 to 4, with dopamine binding exhibiting slightly higher association rate constants overall than DOPA.

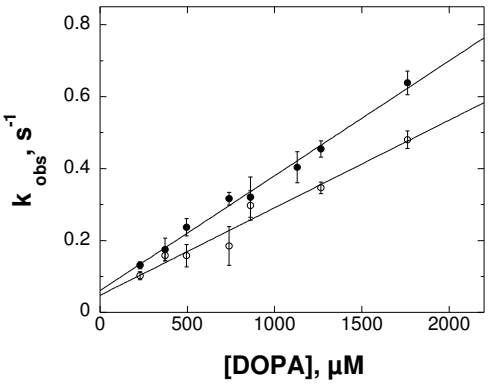


FIGURE 6. Concentration dependence of DOPA binding to $hTyrH_1$ (filled circles) and $hTyrH_4$ (open circles).

While the rate constants for dissociation of catecholamines from TyrH can in principle be determined from the y-intercepts of plots such as those in Figure 6, the precision of the resulting values is low, especially in the case of dopamine. Consequently, the dissociation rate constants were measured directly. This was done by using DHN to displace the bound DOPA or dopamine, taking advantage of the spectral differences between the complexes with DHN, which exhibit maximal absorbance at 550 nm, and those with catecholamines, with maximal absorbance at 690 nm. Each hTyrH isoform (30 µM) was incubated with 60 µM DOPA or dopamine until binding was

complete, as indicated by no further spectral changes. DHN was then added to give a final concentration of 1 mM; this concentration is sufficiently high that all of the catecholamine is displaced by the end of the reaction, and the binding of DHN is much more rapid than the dissociation of the catecholamine (*15*). Under these conditions, the rate constant for the formation of the DHN complex is equal to the rate constant for dissociation of the bound catecholamine. The spectral changes which occur when this is done with DOPA and the unphosphorylated enzymes are illustrated in Figure 7A for $hTyrH_4$. DHN could similarly displace DOPA from the other isoforms. The first order rate constants for dissociation of DOPA from the unphosphorylated isoforms determined in this fashion are summarized in Table 3.

In contrast to the results with DOPA, with dopamine there was no evidence for significant displacement of dopamine by DHN from any of the unphosphorylated isoforms, even after 12 h. There was a slight increase in absorbance at 550 nm, but no accompanying decrease at long wavelength (Figure 7B). At times longer than 12 hours significant protein precipitation was seen. As a result it was not possible to determine the rate constant for dissociation of dopamine from any of the unphosphorylated isoforms. If one assumes that the absorbance change seen in Figure 7B is completely due to replacement of dopamine by DHN and that the spectral changes are identical to those seen with the phosphorylated enzyme (Figure 7C), less than 10% of the dopamine is displaced by DHN after 12 h in the experiment illustrated in Figure 7B. This places an upper limit on the dissociation rate constant of 0.00015 $min^{-1}$.

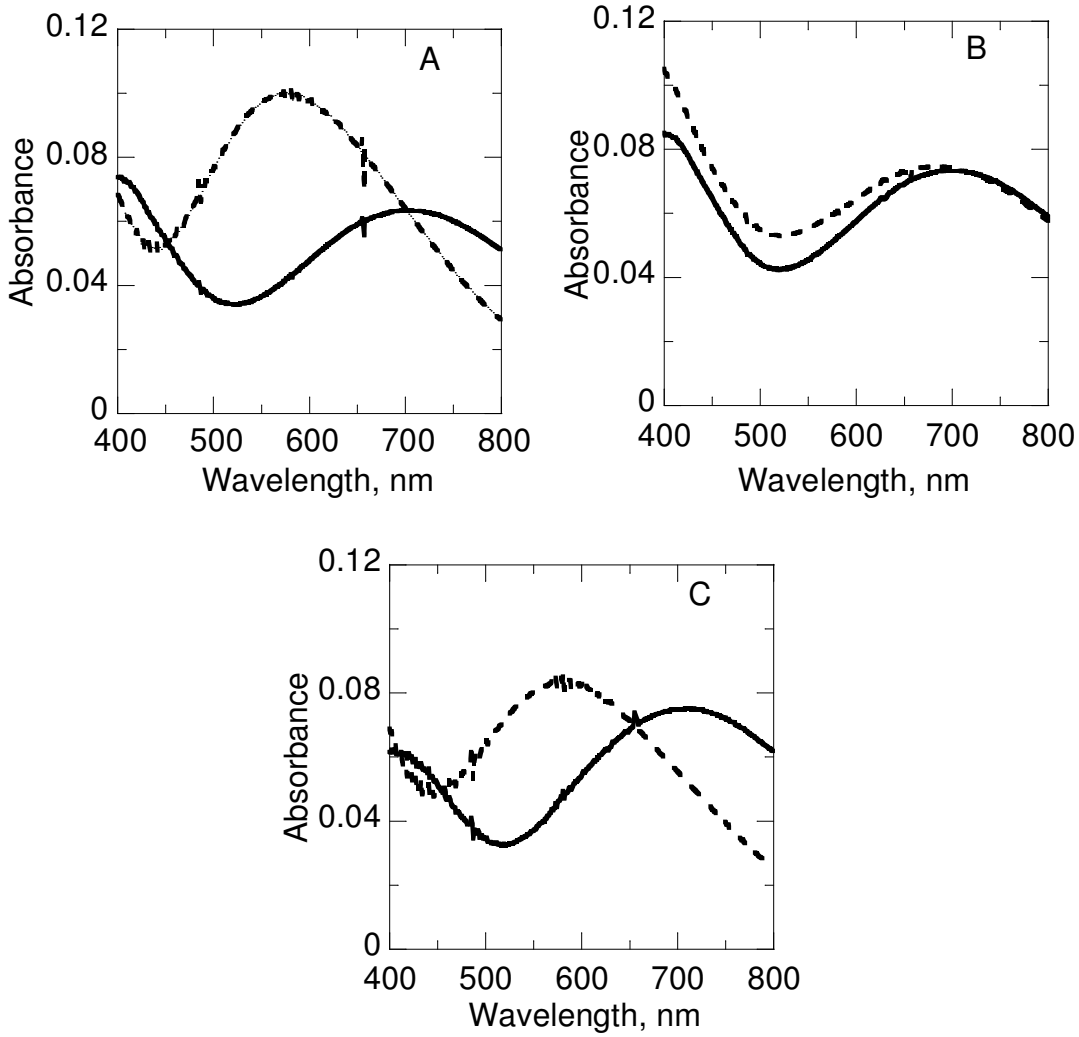


FIGURE 7. Spectral changes during displacement by DHN of DOPA (A) or dopamine (B and C) from unphosphorylated (A and B) and phosphorylated (C) $hTyrH_4$. Enzyme (30 μM) was incubated with 60 μM L-DOPA or dopamine for 15 min in 10% glycerol, 100 mM KCl, and 0.2 mM DTPA, 50 mM HEPES, pH 7, at 10 ºC, before the spectra indicated by solid lines were taken. DHN was then added to give a final concentration of 1 mM; the spectra indicated by dashed lines were taken after 2.8 h (A) or 12.5 h (B and C).

*Effect of phosphorylation by protein kinase A on catecholamine binding to human TyrH.* Each of the TyrH isoforms was phosphorylated with PKA, which is

specific for the serine corresponding to Ser40 of $hTyrH_1$, followed by anion exchange chromatography to remove components of the phosphorylation reaction. When [$\gamma^{32}$P]ATP was used for the reaction, all four hTyrH isoforms were found to be phosphorylated to 0.9 ± 0.2 mol phosphate /mol of enzyme. In addition, no further phosphate could be incorporated into the phosphorylated enzymes by further treatment with PKA and ATP, consistent with stoichiometric phosphorylation. Using the phosphorylated isoforms, the binding and dissociation rate constants for DOPA and dopamine were determined as described above for the unphosphorylated enzymes; the results are summarized in Tables 3 and 4 and illustrated in Figure 8. In the case of DOPA binding, phosphorylation increases the dissociation rate constant by 2.5 to 5-fold and increases the association rate constant by 3 to 4-fold. The increase in the association rate constant is comparable for each isoform, although the absolute magnitude of the value decreases as the size of the regulatory domain increases from $hTyrH_1$ to $hTyrH_4$. As a result of the comparable increases in the association and dissociation rate constants, the change in the $K_d$ value for DOPA varies from an increase of slightly less than two-fold for $hTyrH_1$ to no effect for $hTyrH_4$. Table 3 also shows the much larger increase seen with the rat enzyme (*99*).

In contrast to the very small effect of phosphorylation on the affinity of the human isoforms for DOPA, there is a large effect on the binding of dopamine (Table 4). As was the case with DOPA, phosphorylation increases the association rate constants for all four isoforms by 3 to 4-fold. While no significant displacement of dopamine from the unphosphorylated enzyme could be seen upon incubation with DHN after 12 h, DHN was able to completely displace dopamine from the phosphorylated enzymes over the same time period (Figure 7C). This reflects an increase of at least two orders of magnitude in the dissociation rate constants for dopamine upon phosphorylation. Again, the effect decreases as one progresses from $hTyrH_1$ to $hTyrH_4$. The $K_d$ values for dopamine binding to all four phosphorylated human isoforms are comparable to that for the rat enzyme (*99*).

**Table 3. Kinetic Parameters for DOPA Binding to hTyrH Isoforms.**

| isoform | $k_{on}$[a] ($mM^{-1}$ $min^{-1}$) | $k_{off}$[b] ($min^{-1}$) | $K_d$[c] (μM) |
|---|---|---|---|
| **Unphosphorylated enzyme** | | | |
| **hTyrH$_1$** | 18.6 ± 0.6 | 0.082 ± 0.001 | 4.45 ± 0.16 |
| **hTyrH$_2$** | 17.4 ± 1.2 | 0.078 ± 0.001 | 4.52 ± 0.32 |
| **hTyrH$_3$** | 10.8 ± 0.6 | 0.034 ± 0.001 | 3.17 ± 0.21 |
| **hTyrH$_4$** | 14.4 ± 1.2 | 0.060 ± 0.001 | 4.21 ± 0.36 |
| **rTyrH**[d] | 39.0 ± 3.6 | 0.102 ± 0.006 | 2.70 ± 0.29 |
| **Phosphorylated enzyme** | | | |
| **hTyrH$_1$** | 61.2 ± 2.4 | 0.453 ± 0.012 | 7.41 ± 0.36 |
| **hTyrH$_2$** | 51.6 ± 3.0 | 0.334 ± 0.005 | 6.48 ± 0.40 |
| **hTyrH$_3$** | 40.2 ± 1.8 | 0.235 ± 0.015 | 5.87 ± 0.47 |
| **hTyrH$_4$** | 35.4 ± 1.2 | 0.142 ± 0.002 | 4.02 ± 0.16 |
| **rTyrH**[d] | 66.0 ± 4.8 | 2.76 ± 0.54 | 41.7 ± 13.9 |

[a]Conditions: 10% glycerol, 100 mM KCl, 50 mM HEPES, pH 7, 10 ºC. [b]Conditions: 1 mM DHN, 60 μm DOPA, 10% glycerol, 100 mM KCl, 0.2 mM DTPA, 50 mM HEPES, pH 7, 10 ºC. [c]Calculated from the corresponding $k_{on}$ and $k_{off}$ values. [d]From McCulloch et al. 2001, determined at 15 ºC.

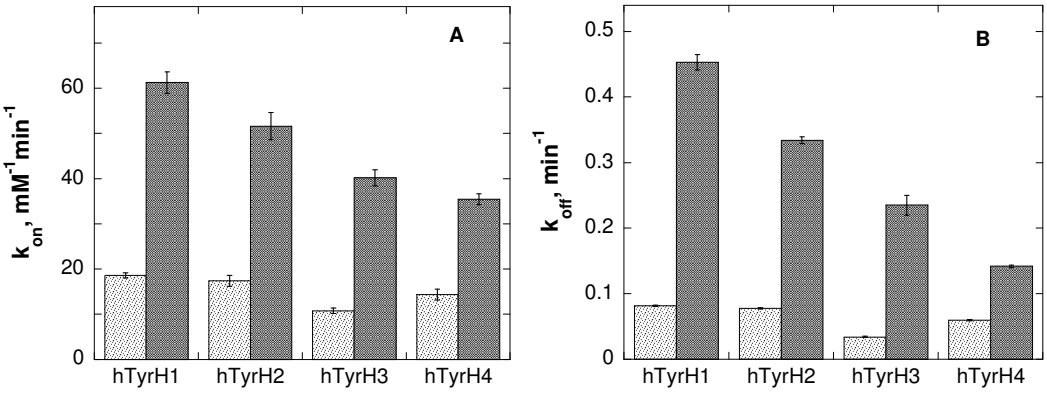


FIGURE 8. Effects of phosphorylation on the rate constants for association (A) and dissociation (B) of DOPA from TyrH isoforms. The conditions were as described for Figure 7.

**Table 4. Kinetic Parameters for Dopamine Binding to hTyrH Isoforms.**

| | Unphosphorylated enzyme | | |
|---|---|---|---|
| isoform | $k_{on}$[a] ($mM^{-1}$ $min^{-1}$) | $k_{off}$[b] ($min^{-1}$) | $K_d$ (nM) |
| **$hTyrH_1$** | 66.6 ± 3.0 | < 0.00015 | < 2.2 |
| **$hTyrH_2$** | 43.2 ± 2.4 | < 0.00015 | < 3.5 |
| **$hTyrH_3$** | 48.6 ± 2.4 | < 0.00015 | < 3.1 |
| **$hTyrH_4$** | 55.2 ± 1.8 | < 0.00015 | < 2.7 |
| **rTyrH**[d] | 312 ± 18 | 0.000041 ± 0.000004 | 0.13 ± 0.02 |
| | **Phosphorylated enzyme** | | |
| **$hTyrH_1$** | 172 ± 7 | 0.024 ± 0.002 | 143 ± 15 |
| **$hTyrH_2$** | 198 ± 7 | 0.016 ± 0.001 | 82 ± 4 |
| **$hTyrH_3$** | 148 ± 7 | 0.012 ± 0.001 | 85 ± 9 |
| **$hTyrH_4$** | 145 ± 4 | 0.011 ± 0.001 | 78 ± 4 |
| **rTyrH**[d] | 474 ± 2 | 0.10 ± 0.002 | 208 ± 20 |

[a]Conditions: 10% glycerol, 100 mM KCl, 50 mM HEPES, pH 7, 10 ºC. [b]Conditions: 1 mM DHN, 60 µm dopamine, 10% glycerol, 100 mM KCl, 0.2 mM DTPA, 50 mM HEPES, pH 7, 10 ºC. [d]From reference (McCulloch et al. 2001); determined at 15 ºC.

## DISCUSSION

The results presented here establish that phosphorylation of human TyrH decreases the affinity of the ferric enzyme for catecholamines and thereby extend the regulatory model developed for the rat enzyme. Still, the human and rat enzymes do show qualitative differences in their regulatory properties, and the four isoforms of human TyrH differ quantitatively in the effects of PKA phosphorylation.

The steady state kinetic parameters of the four human isoforms reported here do not differ substantially from one another, indicating that the different insertions after Met30 of hTyrH do not markedly affect catalysis. The $V_{max}$ values for the different isoforms are comparable and are similar to that of the rat enzyme (*52*), while $hTyrH_1$ has

a slightly higher $K_m$ value for $6MPH_4$ than the other three isoforms. A similar difference in $K_m$ values has been reported using tetrahydrobiopterin as substrate for the human isoforms (*90*). However, when the latter pterin is used, there is substantial substrate inhibition (*90*); this precludes measurement of actual $V_{max}$ values with the physiological substrate, a problem not encountered with $6MPH_4$.

Phosphorylation by PKA of Ser40 in the regulatory domain of rat TyrH greatly decreases the affinity of that enzyme for catecholamines (*15, 91*). The largest effect is on the affinities for dopamine, norepinephrine, and epinephrine, with a smaller effect on the affinity for the product of the TyrH reaction, DOPA. There is no structure available for the regulatory domain of TyrH from any source which would provide insight into the structural basis for this effect. However, there is evidence that phosphorylation alters the structure of the regulatory domain and the interaction between the regulatory and catalytic domains. Phosphorylation increases the sensitivity to trypsin of the residues surrounding Ser40 in the rat enzyme, while dopamine has the opposite effect (*77*), demonstrating that the conformation of this region is sensitive to the regulatory status of the enzyme. The effect of dopamine, which binds in the active site (*100, 101*), on the conformation of the regulatory domain suggests that this region of the regulatory domain is close to the active site. The structure of the combined regulatory and catalytic domains of the related enzyme phenylalanine hydroxylase (*16*), which shows that the N-terminus of the regulatory domain physically blocks the active site, supports such a model. The insertions found in $hTyrH_2$, $hTyrH_3$ and $hTyrH_4$ are after Met30 and thus immediately precede the phosphorylation sensitive region, providing a link between the structural differences among the human isoforms and any differences in their response to phosphorylation.

Clearly, dopamine binds very tightly to all four human isoforms. In the case of the unphosphorylated enzyme, dopamine binding is effectively irreversible. For all four isoforms, phosphorylation results in an increase in the rate constants for dopamine dissociation of at least two orders of magnitude, with much smaller increases in the rate constants for association. Qualitatively this resembles the effects of phosphorylation of

the rat enzyme, demonstrating that the regulatory model developed with rat TyrH (Scheme 4) also applies to the human isoforms. In addition, there are quantitative differences in the binding of dopamine to the different phosphorylated isoforms. There is a small decrease in the association rate constant as one progresses from $hTyrH_1$ to $hTyrH_4$ for both the unphosphorylated and phosphorylated enzymes. A more significant effect is seen on the dissociation rate constants for the phosphorylated enzymes, which decrease as the size of the insertion after Met30 increases. As a result of these two trends, phosphorylated $hTyrH_1$ has a significantly lower affinity for dopamine than the other three isoforms. Whether the same trend is seen with the unphosphorylated enzyme cannot be determined from the present data, although the results with DOPA (*vide infra*) suggest that this is indeed the case. However, the data do establish that the effect of phosphorylation on dopamine binding is attenuated by the insertions.

The effects of phosphorylation on binding of DOPA to the human isoforms differ significantly from the effects on the binding of dopamine. The DOPA association and dissociation rate constants both decrease slightly as the size of the insertion increases from $hTyrH_1$ to $hTyrH_4$, resulting in the $K_d$ values for DOPA binding to the unphosphorylated enzymes being essentially identical for all four isoforms and close to the value for the rat enzyme. However, phosphorylation by PKA has little to no effect on the affinity of human TyrH for DOPA. The association rate constants for all four isoforms increase about 4-fold upon phosphorylation; this is greater than the increase seen with the rat enzyme (*15*), but comparable to the change in the association rate constants for dopamine binding to the human enzymes. The increases upon phosphorylation in the rate constants for DOPA dissociation from the human isoforms are much less than is seen for rat TyrH. As was the case for dopamine binding, the insertions attenuate the effects of phosphorylation, in that both the association and dissociation rate constants for DOPA show smaller increases upon phosphorylation as the size of the insertion increases. Because both rate constants increase by comparable amounts, the $K_d$ values increase less than two-fold when $hTyrH_1$ is phosphorylated. The effect of phosphorylation on the $K_d$ value decreases as the size of the insertion increases,

to the point where the value for $hTyrH_4$ shows no change upon phosphorylation. In contrast, upon phosphorylation of rat TyrH the $K_d$ value for DOPA increases about 20-fold.

The lack of a substantial change in the affinity of hTyrH for DOPA upon phosphorylation suggests that inhibition of the human enzyme by DOPA is not important for regulation in vivo while inhibition by dopamine is. This observation would be consistent with physiological levels of the two inhibitors. The concentration of DOPA in brain and adrenal tissues is quite low, well below 1 μM, due to its rapid conversion to dopamine by DOPA decarboxylase (*102-105*). Thus, the $K_d$ for DOPA for even unphosphorylated hTyrH is likely to be much higher than the physiological concentration. This suggests that even unphosphorylated TyrH is not significantly inhibited by DOPA in the cell. In contrast, the average concentration of dopamine in brain and adrenal tissue is 5-10 μM (*102, 104, 105*); the concentration in the cytosol is undoubtedly much lower, since most of the dopamine is inside secretory vesicles (*106-108*). The much lower $K_d$ value for dopamine for the phosphorylated isoforms is consistent with the much lower level of catecholamines in the cytosol. Moreover, when TyrH is isolated from bovine adrenal or rat pheochromocytoma cells, the enzyme has a combination of dopamine, epinephrine, and norepinephrine bound, but no DOPA (*92, 93*). This lack of DOPA in enzyme isolated from physiological sources is consistent with it not being a physiologically important inhibitor.

In conclusion, the data presented here show that the regulatory model developed for rat TyrH also applies to all four human isoforms. The human isoforms differ from the rat enzyme in the lack of an effect of phosphorylation on DOPA binding. In addition, the insertions in the regulatory domain which differentiate the four human isoforms do affect their regulatory properties.

# CHAPTER III

# MONITORING THE MOVEMENT OF THE LOOP RESIDUES 175-200 IN RAT TYROSINE HYDROXYLASE BY FLUORESCENCE ANISOTROPY

## INTRODUCTION

TyrH catalyses the rate-limiting step in catecholamine synthesis, the hydroxylation of tyrosine to form DOPA with concomitant oxidation of pterin using molecular oxygen (*81*). The crystal structures of complexes of the homologous enzyme phenylalanine hydroxylase (PheH) with tetrahydrobiopterin and with both tetrahydrobiopterin and 3-(2-thienyl)-alanine show a large movement of a surface loop (residues 131-155) at the active site opening upon amino acid binding (Figure 9) (*22*). So far only two crystal structures for rTyrH are known; one with no ligands (*17*) and one with bound 7,8-dihydrobiopterin (*18*). The overall structure of catalytic domain does not change upon pterin binding. The loop region can be identifiable with missing residues between 182 and 186. There is no structure of TyrH or PheH with only an amino acid bound. The ternary structure of PheH shows a large conformational change in the surface loop upon binding of amino with most the moved residue being Tyr138 (Figure 9B). This opens the question of whether a conformational change in the TyrH residues175-200 corresponds to the movement of PheH loop residues 131-155 (Figure 9A and 10). Alanine scanning mutagenesis of these loop residues in TyrH shows that the $K_{6MePH4}$ value does not change, whereas $K_{tyr}$ and DOPA formation decrease and coupling between pterin oxidation and amino acid hydroxylation also decreases towards the center of loop. These results indicate that the loop plays an important role in DOPA formation (Daubner-unpublished observations). In the present study, steady-state and frequency-domain time-resolved fluorescence anisotropy spectroscopy were used to monitor movement of the loop in TyrH upon ligand binding.

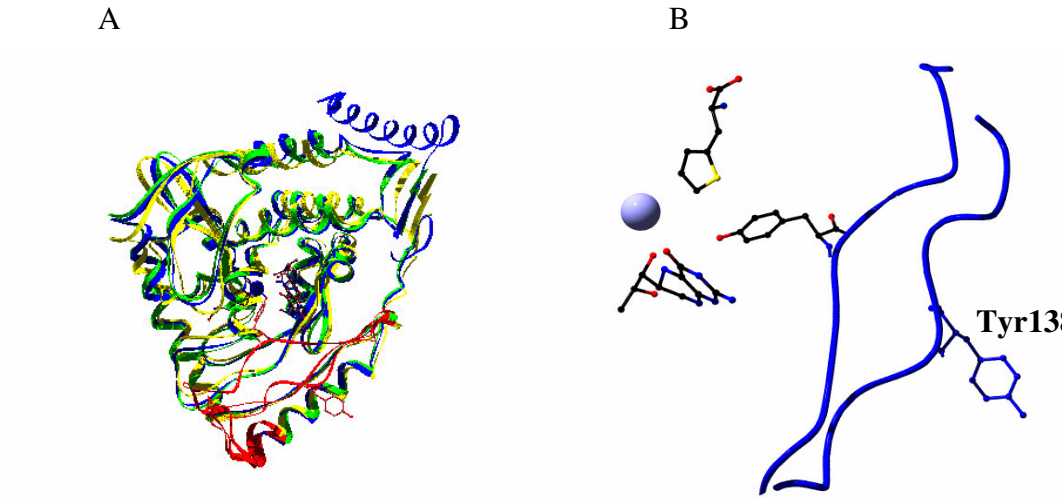


FIGURE 9. (A) The structures of hPheH with $BH_4$ bound (from PDB file 1J8U-green), hPheH with both $BH_4$ and thienylalanine bound (from PDB file 1KW0-yellow) and of rTyrH with 7,8-$BH_2$ bound (from PDB file 2TOH-blue) with loops shown in pink. (B) The movement of the 130-150 loop in PheH when an amino acid is bound.

```
TyrH   CHHLVTKFDPDLDLDHPGFSDQVYRQR
PheH   FANQILSYGAELDADHPGFKDPVYRAR
```

FIGURE 10. Sequence alignment of PheH residues (131-155) and TyrH residues (177-203) loop regions.

## EXPERIMENTAL PROCEDURES

*Materials.* Custom oligonucleotides were obtained from Integrated DNA Technologies (Coralville, IA). Restriction endonucleases were from New England Biolabs Inc (Beverly, MA). *Pfu* DNA polymerase was obtained from Stratagene USA (La Jolla, CA). DNA sequencing was performed using the BigDye kit of ABI (Foster City, CA). 6-Methyltetrahydropterin ($6MePH_4$) were purchased from B. Schircks Laboratories (Jona, Switzerland). Leupeptin and pepstatin were obtained from Peptides International (Louisville, KY). Catalase was obtained from Roche (Gaithersburg, MD). Distilled glycerol was from Invitrogen (Carlsbad, CA). 6-Methyl-5-

deazatetrahydropterin was synthesized essentially as described by Moad et al. (*109*) by Dr. Vijay Gawandi of Texas A&M University. All other reagents were commercially available.

*Cloning and characterization of tryptophan mutants.* The three tryptophan residues at positions 166, 233, and 372 of rat TyrH were mutated sequentially to phenylalanine using the oligonucleotides in Table 5 using the Quick-Change protocol. In addition, Phe184 was mutated to tryptophan. These mutants were expressed in *E. coli* BL21 Star (DE3) cells as previously described for wild type TyrH (*76*); an AKTA FPLC with a 5 ml Hitrap-Heparin column was used in place of the Heparin-Sepharose column. The protein was dialyzed against 50 mM HEPES, pH 7.0, 10% glycerol and 75 µM diethylenetriaminepentaacetic acid (DTPA) prior to being loaded onto the Hitrap-Heparin column; this was eluted with a linear gradient of 0-0.8 M NaCl in 75 µM DTPA, 10% glycerol, 50 mM HEPES, pH 7.0. Fractions containing tyrosine hydroxylase were pooled and precipitated by making the solution 65% saturated in ammonium sulfate. The pellet was resuspended in 100 mM KCl, 10% glycerol, 1 µM pepstatin, 1 µM leupeptin, 50 mM HEPES, pH 7.0 to give a concentration of ~300 µM TyrH. To this, ferrous ammonium sulfate was added to give a 20% molar excess of iron over TyrH active sites; excess iron was removed by dialysis (*91*). All protein purification steps were carried out at 4 ºC. Purified enzymes were stored at -80 ˚C. To obtain apoenzyme, the 65% ammonium sulfate pellet was dissolved in the same buffer containing 1 mM EDTA and incubated on ice for 30 minutes. The enzyme was then dialyzed against the same buffer to remove excess EDTA. The final stoichiometry of iron:enzyme was determined by atomic absorption spectroscopy on a Perkin Elmer AAnalyst. All the enzymes used in this study contained 0.9-1.2 equivalents of iron in the holoenzyme or less than 0.2 equivalents in the apoenzyme.

**Table 5. Oligonucleotides Used for Construction of Expression Plasmids for Tryptophan Mutants.**

| Mutation | Plus strand | Minus strand |
|---|---|---|
| W166F | 5'-CAAGGTCCCCTTTTTCCC GCGGAAAGTG-3' | 5'-CACTTTCCGCGGGAAAAA GGGGACCTTG-3' |
| F184W | 5'-CCTGGTCACCAAGTGGG ACCCTGATCTGG-3' | 5'-CCAGATCAGGGTCCCACT TGGTGACCAGG-3' |
| W233F | 5'-GGAAGAGATTGCTACCT TTAAGGAGGTATATGTCAC GC-3' | 5'-GCGTGACATATACCTCCT TAAAGGTAGCAATCTCTTC C-3' |
| W372F | 5'-CCACGGTGTACTTTTTCA CTGTGG-3' | 5'-CCACAGTGAAAAAGTACA CCGTGG-3' |

*Enzyme assays:* A colorimetric end point assay for DOPA formation was used to measure tyrosine hydroxylase activity (*52*). Standard conditions were 0.5 μM enzyme, 400 μM $6MePH_4$ and 100 μM tyrosine in 50 mM HEPES, pH 7.0, 100 μg/ml catalase, 1 mM dithiothreitol, 10 μM ferrous ammonium sulfate, at 25 ºC. For determination of the $K_m$ value for tyrosine, assays contained 400 μM $6MePH_4$ and 10 to 360 μM tyrosine. For determination of the $K_m$ value for $6MePH_4$, assays contained 100 μM tyrosine and 10 to 360 μM $6MePH_4$. To obtain the kinetic parameters in Table 6, the kinetic data were fit to the Michaelis-Menten equation using the program KaleidaGraph (Synergy Software). Inhibition data obtained by $6M5DPH_4$ were fit to the competitive inhibitor equation using Igor Pro program (WaveMatrics, Inc.).

Rates of formation of tyrosine from phenylalanine were measured by monitoring the increase in absorbance at 275 nm (*26, 110*). The conditions were 0.4 μM enzyme, 200 μM $6MePH_4$, 25 mM EPPS, pH 7.0, 60 μg/ml catalase, 10 μM ferrous ammonium sulfates and 5mM DTT. Rates of pterin oxidation were measured in the presence of phenylalanine as substrate for W166F/F184W/W233F/W372F TyrH by a coupled assay with dihydropteridine reductase, monitoring the decrease in absorbance at 340 nm due to

NADH oxidation. The background rate due to auto oxidation of the tetrahydropterin was subtracted when calculating the rate of the enzymatic reaction. Conditions were 0.4 μM enzyme, 400 μM $6MePH_4$, 100 μg/ml catalase, 25 mM EPPS, pH 7.0, 10 μM ferrous ammonium sulfate, 0.2 mM NADH, 0.25 units/mL sheep dihydropteridine reductase (DHPR) at 25˚C with varying concentration of phenylalanine from 0.5-12.6 mM.

*Steady-state fluorescence intensity and anisotropy.* Steady-state fluorescence intensity and anisotropy were measured on an ISS Koala Model fluorometer equipped with a xenon arc lamp. Light of 300 nm wavelength was selected from the source by a monochromator and passed through a 0.5 mm slit and a Glan Thompson vertical polarizer. The emitted fluorescence between 310 and 500 nm wavelength range was collected through a 1.0 mm slit. For anisotropy measurements, emission intensities were collected through a 2 mm thick Schott WG345 cut-on filter and a Glan Thompson polarizer. The intensity from the samples upon addition of $6M5DPH_4$ was corrected with a factor for the inner filter effect, obtained by titrating $6M5DPH_4$ against N-acetyl-L-tryptophanamide (NATA). NATA is an analogue for tryptophan in protein. All fluorescence studies were performed in 25 mM EPPS, pH 7.0, with a blank correction of the buffer. A W166F/F184W/W233F/W372F TyrH concentration of 3 μM was used for all steady-state fluorescence measurements.

*Frequency-domain lifetime and anisotropy measurements.* Frequency-domain measurements were performed on an ISS K2 multifrequency fluorometer equipped with digital acquisition electronics and fast Fourier transform data processing capability. The excitation beam of a 300 nm line from a Spectra Physics model argon ion laser was selected by passing through a Melles Griot-FIU004 filter which removes the 275 nm line produced by a deep-UV mode. The 300 nm line from the laser is always vertically polarized. Samples of 12 μM W166F/F184W/W233F/W372F TyrH in 25 mM EPPS, pH 7.0 were excited by the 300 nm modulated line and the modulated emission was passed through Glan Thompson polarizer. The ligands were dissolved in the same buffer. For lifetime measurements, emission was observed through the polarizer oriented at 54.7° to the vertical axis to avoid polarization artifacts. Phase shift and modulation data for each

sample with reference to NATA were obtained at each frequency of excitation. NATA with a lifetime of 2.85 ns in 0.1 M phosphate buffer, pH.7, was used as a reference sample. For frequency-domain anisotropy measurements, the emission was observed through the polarizer which is rotated between parallel and perpendicular orientation. The differential phase shift was obtained from the difference between the perpendicular and parallel components of the emission, and the modulation ratio was obtained from the ratio of the parallel to the perpendicular components of the modulated emission. Data analysis of lifetime measurements was performed by fitting the data to a Gaussian distribution of lifetimes (equation 11) using Globals Unlimited software from the Laboratory for Fluorescence Dynamics, University of Illinois. The differential phase angle and modulation ratio data obtained frequency-domain experiment, were fit to a model described by equation 9 for a hindered local rotation with a slow global rotation using same software.

*General principles of fluorescence anisotropy.* Anisotropy represents a means to monitor rotations of macromolecules in solution using the intrinsic fluorescence of the macromolecule itself or the extrinsic fluorescence of an attached probe. Anisotropy is the ratio of the polarized component to the total intensity (equation 2). It is measured by exciting a sample with vertically polarized light and measuring the subsequent emission through a polarizer oriented either parallel to the direction of polarized excitation ($I_{\parallel}$) or perpendicular to the direction of polarized excitation ($I_{\perp}$). Anisotropy (r) is expressed by equation 2.

$$r = \frac{I_{II} - I_{\perp}}{I_{\perp} + 2I_{\mathrm{II}}} \qquad (2)$$

For a fluorophore which is immobile during the lifetime of its excited state, the anisotropy $r_0$ is given by equation 3. Here $\beta$ is angle between absorption and emission dipoles. Anisotropy measured from fluorescence is between 0.4 and -0.2 because of photoselection upon excitation, non parallel absorption-emission dipoles and rotation of the molecule during the lifetime of excited state. Rotation of a fluorophore, resulting either from global movements of the macromolecule to which it is attached or to local

motions at the point of attachment, will lead to depolarization subsequent to absorption, as described by the Perrin equation 4 (*111*). Here $r_0$ is the anisotropy in the absence of rotational diffusion, τ is the lifetime of the fluorophore, and θ is the correlation time for the diffusion process in the steady-state, an average of global and local rotational correlation times. Rotational correlation times for a hypothetical spherical protein may be related to physical constants as by equation 5 (*111, 112*). Here, η is the viscosity of the solution, k is the Boltzman constant, T is absolute temperature and V is the volume of the rotating unit.

$$r_0 = \frac{2}{5}\left[\frac{3\cos^2\beta - 1}{2}\right] \qquad (3)$$

$$r = \frac{r_0}{1 + (\tau/\theta)} \qquad (4)$$

$$\theta = \frac{\eta V}{kT} \qquad (5)$$

*General principle of frequency-domain measurements of lifetime.* In order to determine explicitly fluorescence decay rates, time-resolved techniques must be used rather than the steady-state measurements described above. For time resolved anisotropy, there are two methods: i) time-domain and ii) frequency-domain. The time-domain, pulse or impulse response method involves exciting a sample with a short burst of vertically polarized light and measuring the subsequent decay of fluorescence intensity along parallel and perpendicular orientations. Here, only frequency-domain will be discussed. The frequency-domain, phase-modulation or harmonic response approach involves a sample which is continuously excited by vertically polarized light whose intensity is modulated sinusoidally at an angular frequency ω. Because of the lag time between absorption and emission, the emission with the same frequency is delayed in time relative to excitation, resulting in a phase shift and demodulated emission. The phase shift is the fraction of a complete cycle elapsed as measured from an excitation reference point and often expressed as an angle. Modulation is the ratio of the amplitude of an emission wave to an excitation wave. With increasing modulation frequency of

excitation, the phase shift increases from 0° to 90° and the modulation decreases from 1.0 to 0.0. The relationship at each frequency between the phase shift (Φ) and the modulation ratio (m) and lifetime (τ) is given by equations 6 and 7 (*113*). Here, $\tau_\Phi$ and $\tau_m$ are the lifetimes calculated from the phase shift and from the modulation ratio, respectively. $\tau_\Phi$ and $\tau_m$ will only be equal to each other and invariant with frequency if the sample is homogeneous (*113*). Even though the equations help in calculating lifetimes directly, usually lifetime measurements are done by measuring the phase shift and modulation with reference to a sample of known lifetime. Data from the sample and from the reference are collected at several frequencies of excitation. At each frequency, the extent of demodulation and the phase shift produced by the sample of unknown lifetime are measured. This can allow the modeling of more complex emission mechanism the might give rise to multiple exponential decays or distributions of many closely spaced lifetimes.

$$\tan\phi = \omega\tau_\phi \qquad (6)$$

$$m = \frac{1}{\sqrt{1+\omega^2\tau_m^2}} \qquad (7)$$

*General principle of frequency-domain measurements of dynamic anisotropy.* Dynamic anisotropy or differential polarization can be determined by phase-modulation fluorometry. The differential phase shift of perpendicular and parallel components of emission and demodulation ratio of the parallel to perpendicular components of emission from a sample are measured subsequent to excitation with polarized sinusoidally-modulated light (*114, 115*). The primary advantage of dynamic anisotropy over the steady-state method is the ability to separate and quantify the different modes of rotation (equation 8). Because of the complex nature of the equations describing the response of differential phase and modulation to variations in rotational characteristics, simulations are typically performed. For example, a tryptophan on a protein may posses rotational characteristics deriving from the motion of the protein as a whole as well as faster motions associated with the side chain itself (*116, 117*). The rate of anisotropy decay is given by equation 9. Here $r_0$ is the anisotropy at time t = 0, $r_\infty$ is the anisotropy that

persists at times long relative to the short correlation time, $\theta_1$. $\theta_2$ is the rotational correlation time for the slower global rotation, and $\theta_1$ is the rotational correlation time for the hindered local rotation. Therefore, dynamic anisotropy measurements when performed at multiple frequencies not only have the capability of assigning separate rotational correlation times to each level of rotational motion, but also can differentiate at the local level between the amplitude and rates of rotation associated with the side chain. Changes in the amplitude of local motion, for example, are reflected as changes in $r_\infty$ in equation 9, while changes in the rates of motion are represented by changes in $\theta_1$. Steady-state measurements of anisotropy can present at best an average of all such processes. The amplitude of local motion may be described in terms of a cone angle of limited rotation ($\Phi$) by equation 10.

$$r(t) = \sum_i r_i e^{-t/\theta_i} \qquad (8)$$

$$r(t) = [(r_0 - r_\infty)e^{-t/\theta_1} + r_\infty]e^{-t/\theta_2} \qquad (9)$$

$$\text{or } r(t) = (r_0 - r_\infty)e^{-t/\theta_1} + r_\infty e^{-t/\theta_2}$$

$$\cos(\Phi) = \left[\left(1 + 3\left(\frac{r_\infty}{r_0}\right)^{1/2}\right)^{1/2} - 1\right] \qquad (10)$$

**RESULTS**

*Cloning and characterization of tryptophan mutants.* TyrH has tryptophans at positions 166, 233 and 372. To avoid the complications associated with fluorescence anisotropy measurements, these tryptophans were mutated to phenylalanine. The residue Phe184 in the center of loop was mutated to tryptophan to monitor the movement of loop. All mutant proteins expressed well in *E. coli* and could be purified using the protocol developed for the rat enzyme. After incubation with a slight excess of ferrous ammonium sulfate and removal of excess iron, each mutant contained one atom of iron per monomer. Apoenzyme contained less than 0.2 equivalent iron per monomer. The

steady state kinetic parameters with tyrosine and $6MePH_4$ as substrates were measured for all tryptophan mutants and are summarized in Table 6. In the case of W166F mutations, the $K_{6MePH4}$ value increased 3 to 4 fold. In the cases of W372F and F184W/W372F TyrH the $K_{tyr}$ value decreased 5 to 10 fold. Otherwise the kinetic parameters suggest that catalysis and binding are not significantly perturbed in these mutant proteins (Table 6).

**Table 6. Steady State Kinetic Parameters of TyrH Tryptophan Mutants.**

| Enzyme | $K_{tyr}$ ($\mu M$)[a] | $K_{6MePH4}$ ($\mu M$)[b] | $V_{max}$ ($min^{-1}$) |
|---|---|---|---|
| WT rTyrH | 80 ± 18 | 45 ± 4 | 182 ± 26 |
| W372F rTyrH | 8 ± 1 | 45 ± 5 | 44 ± 3 |
| W166F/W372F rTyrH | 90 ± 4 | 180 ± 18 | 243 ± 5 |
| W166F/W233F/W372F rTyrH | 90 ± 6 | 162 ± 15 | 276 ± 7 |
| W166F/F184W/ W233F/W372F rTyrH | 64 ± 6 | 116 ± 11 | 165 ± 5 |
| W166F/F184W/W372F rTyrH | 65 ± 5 | 129 ± 4 | 184 ± 5 |
| F184W/W372F rTyrH | 17 ± 5 | 31 ± 4 | 64 ± 6 |

Conditions: 0.2 μM enzyme, 100 μg/ml catalase, 50 mM HEPES, pH 7.0, 10 μM ferrous ammonium sulfate, 1 mM DTT at 25˚C. [a]380 μM $6MePH_4$ with varied concentrations of tyrosine from 0-350 μM. [b]100 μM tyrosine with varied concentrations of $6MePH_4$ from 0-350 μM

Phenylalanine is a known substrate for TyrH (*23*). The steady state kinetics for tetrahydropterin oxidation and tyrosine formation by W166F/F184W/ W233F/W372F rTyrH were studied as described in Experimental Procedures. The data for tetrahydropterin oxidation were fit to the Michaelis-Menten equation to yield a $K_{phe}$ value of 0.90 ± 0.04 mM and a $V_{max}$ value of 264 ± 4 $min^{-1}$ (Figure 11A). A $K_{phe}$ value of 0.90 ± 0.16 mM and a $V_{max}$ value of 55 ± 3 $min^{-1}$ were obtained for tyrosine formation

(Figure 11B). These results indicate that only 20% of $6MePH_4$ oxidation was used for tyrosine formation.

$6M5DPH_4$ is an air stable analogue of the substrate $6MePH_4$ (Figure 12). Accordingly, the deazapterin was used to study binding to the pterin binding site (*118*). $6M5DPH_4$ is a competitive inhibitor *vs* $6MePH_4$ with a $K_i$ value of 140 ± 19 μM (Figure 13).

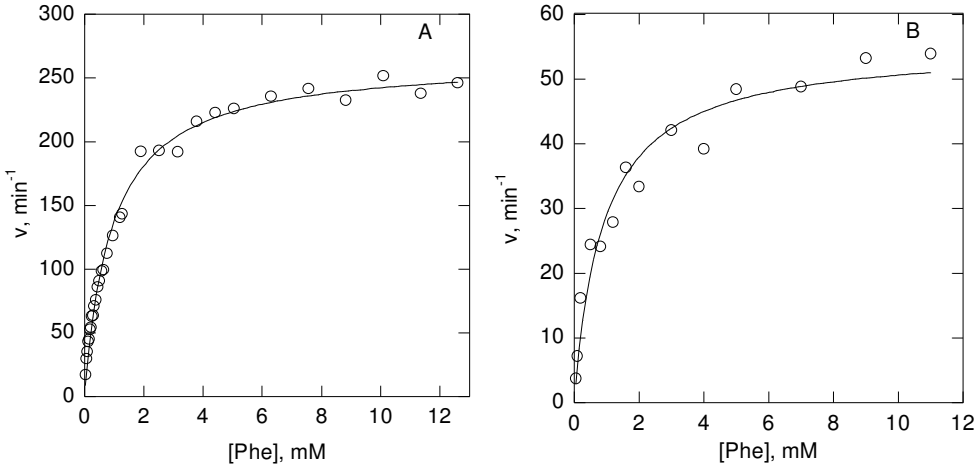


FIGURE 11. Steady state kinetics of W166F/F184W/W233F/W372F rTyrH with phenylalanine as a substrate. A) tetrahydropterin oxidation; B) tyrosine formation. Conditions were as described in Experimental Procedures. The lines are from fits to the Michaelis-Menten equation.

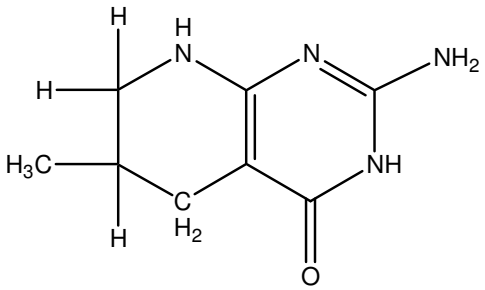


FIGURE 12. 6-Methyl-5-deazatetrahydropterin ($6M5DPH_4$).

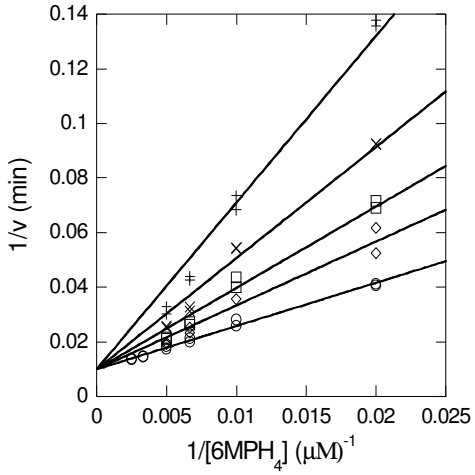


FIGURE 13. Inhibition of W166F/F184W/W233F/W372F TyrH by $6M5DPH_4$. Initial rates were determined in the presence of no (○), 50 μM (◊), 100 μM (□), 200 μM (x), or 400 μM (+) $6M5DPH_4$. The lines are from v = (VS)/( $K$(1 + I/$K_s$) +S). Conditions: 0.5 μM W166F/F184W/W233F/W372F TyrH, 25 μM EPPS pH 7.0, 0.2 mM NADH, 2.5 μl dihydropteridine reductase (, 100 μg catalase, 10 μM $Fe(NH_4)_2SO_4$.

*Steady state fluorescence intensity.* The intrinsic tryptophan fluorescence emission from the enzyme was determined in the presence and absence of ligands. The corrected intensity of W166F/F184W/W233F/W372F TyrH in the presence of either phenylalanine or $6M5DPH_4$ was not significantly different from that in the absence of these ligands (Figure 14).

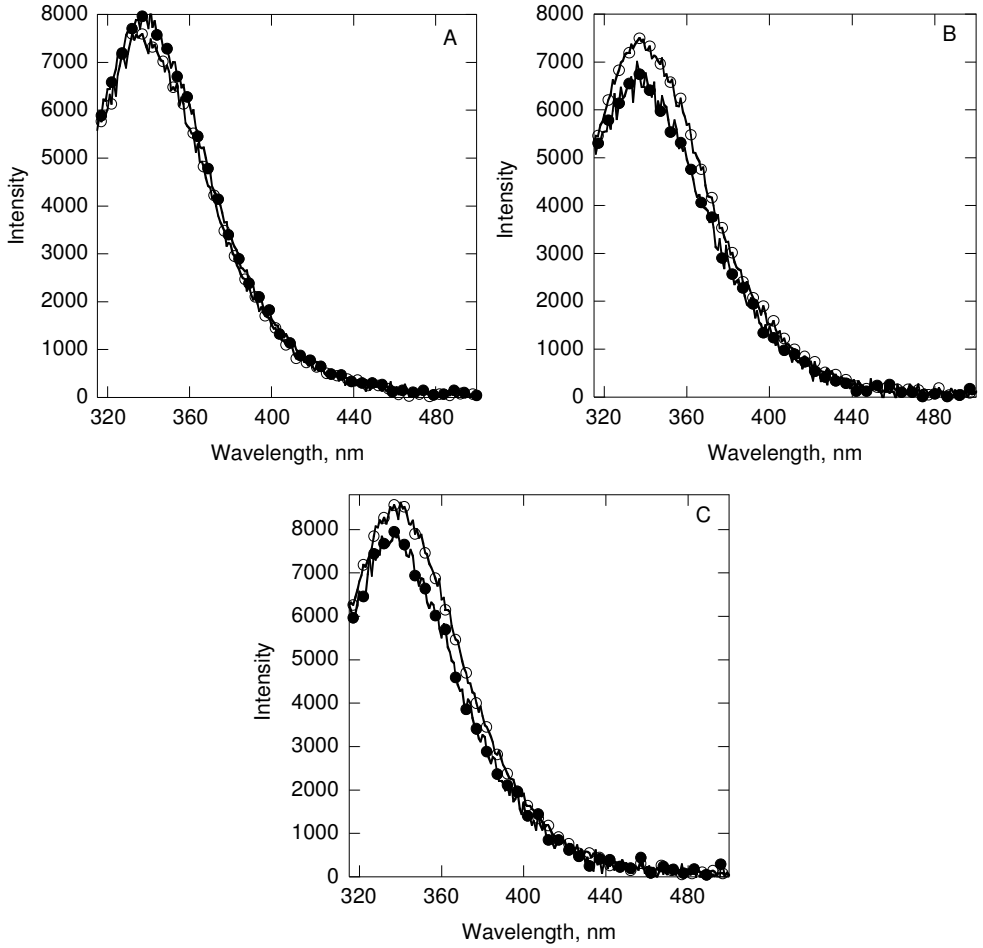


FIGURE 14. Steady state fluorescence intensity of W166F/F184W/W233F/W372F rTyrH (FeIII) in 25 mM EPPS buffer, pH 7.0, at 25 ºC in the absence (○) and presence (●) of (A) 10 mM phenylalanine, (B) 500 µM 6M5DPH$_4$, or (C) both ligands.

*Steady-state fluorescence anisotropy of W166F/F184W/W233F/W372F TyrH in the presence of ligands.* Steady-state fluorescence anisotropy is a measurement for the movement of an intrinsic fluorophore. The steady-state fluorescence anisotropy of the single tryptophan in the protein was measured by exciting the sample with plane polarized light of 300 nm oriented vertically and recording the emission intensity passing through an emission filter of Schott WG345 and Glan Thompson polarizer oriented vertical and horizontal to the excitation light. The average anisotropy of W166F/F184W/W233F/W372F TyrH with iron bound is 0.177 ± 0.001 in the absence of ligands. The steady state anisotropy experiments with the $6M5DPH_4$ were performed at 500 μM to avoid an inner filter effect, although this concentration is not saturating. The anisotropy increases in the presence of either phenylalanine or $6M5DPH_4$ (Figure 15). A much larger increase in anisotropy is observed with $6M5DPH_4$ alone than with phenylalanine alone (Figure 15). The increase in anisotropy is concentration dependent for both phenylalanine and $6M5DPH_4$ (Figure 16). In case of phenylalanine, the observed anisotropy upon addition of 10 mM at a time is much than the anisotropy change upon titration. The $K_d$ values determined from the anisotropy of 0.73 ± 0.30 mM for phenylalanine and 224 ± 44 μM for $6M5DPH_4$ are comparable to the steady-state kinetic $K_{phe}$ and $K_i$ values. The presence of phenylalanine results in a similar $K_d$ value of 190 ± 34 μM for $6M5DPH_4$ and an increase in anisotropy of 0.001 ± 0.003 (Figure 16C). Essentially all of the change in anisotropy of 0.015 ± 0.002 is observed with $6M5DPH_4$ alone (Figure 15B and 17C).

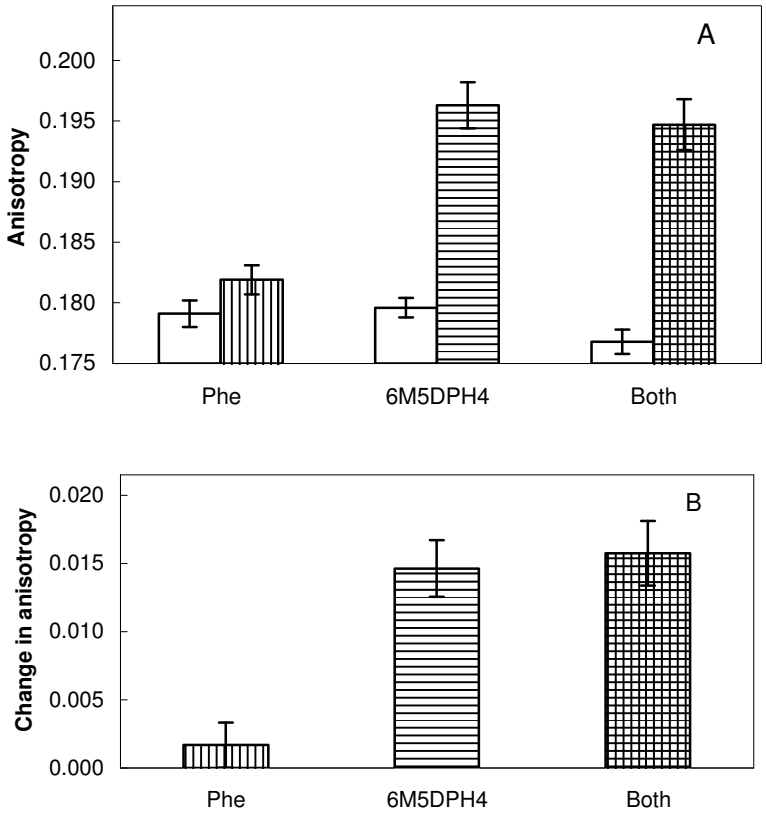


FIGURE 15. Steady-state fluorescence anisotropy of W166F/F184W/W233F/W372F rTyrH (FeIII) in 25 mM EPPS buffer, pH 7, at 25 ºC: (A) in the absence (empty bars) and presence (filled bars) of 10 mM phenylalanine and 500 µM $6M5DPH_4$. (B) Change in anisotropy.

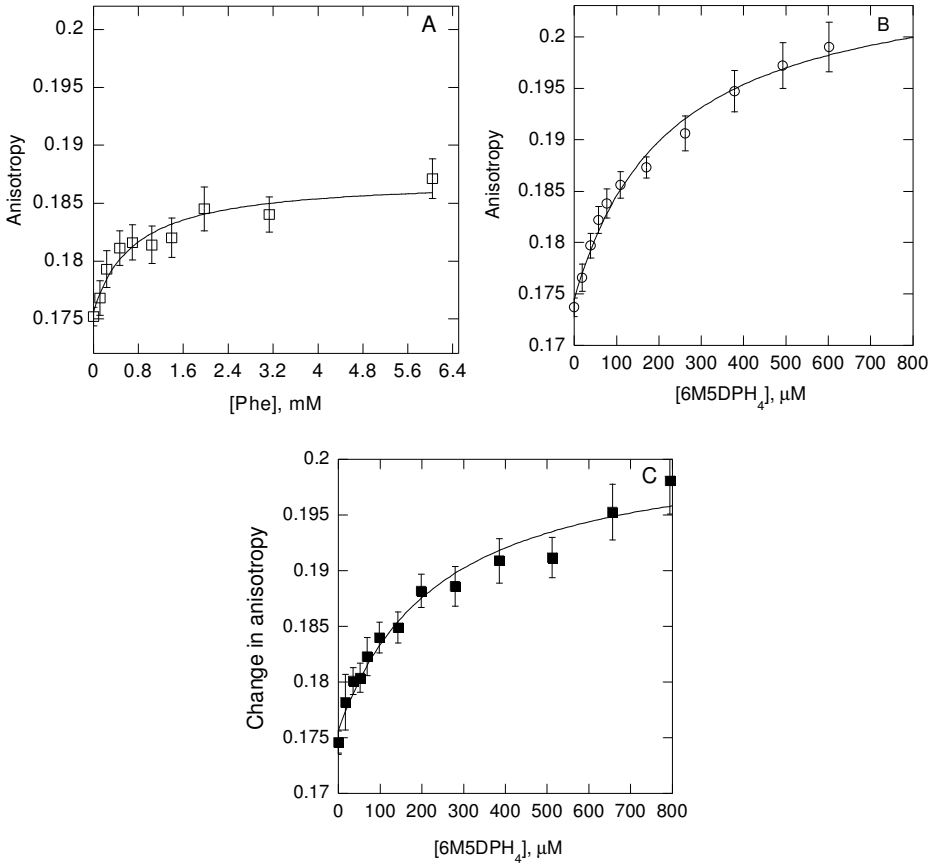


FIGURE 16. Steady-state fluorescence anisotropy of W166F/F184W/W233F/W372F rTyrH Fe(III) in 25 mM EPPS buffer, pH 7, at 25 ºC as a function of the concentration of (A) phenylalanine (□), (B) 6M5DPH$_4$ (○), or (C) 6M5DPH$_4$ in the presence of 10 mM phenylalanine (■).

The magnitude of the anisotropy change also depends on whether the enzyme contains iron (Figure 17). In case of the apoenzyme the average anisotropy was 0.1572 ± 0.0008 whereas holoenzyme was 0.1768 ± 0.0009. Titration of the apoenzyme with ferric iron to make holoenzyme was not possible because of its insolubility. The addition of phenylalanine resulted in a decrease in the anisotropy of the apoenzyme. Addition of 6M5DPH$_4$ increased the anisotropy by 0.010 ± 0.002, while the presence of both ligands increased it somewhat less, to 0.007 ± 0.002 (Figure 17 A and B). These magnitudes were less than the increases seen with the holoenzyme (Figure 18).

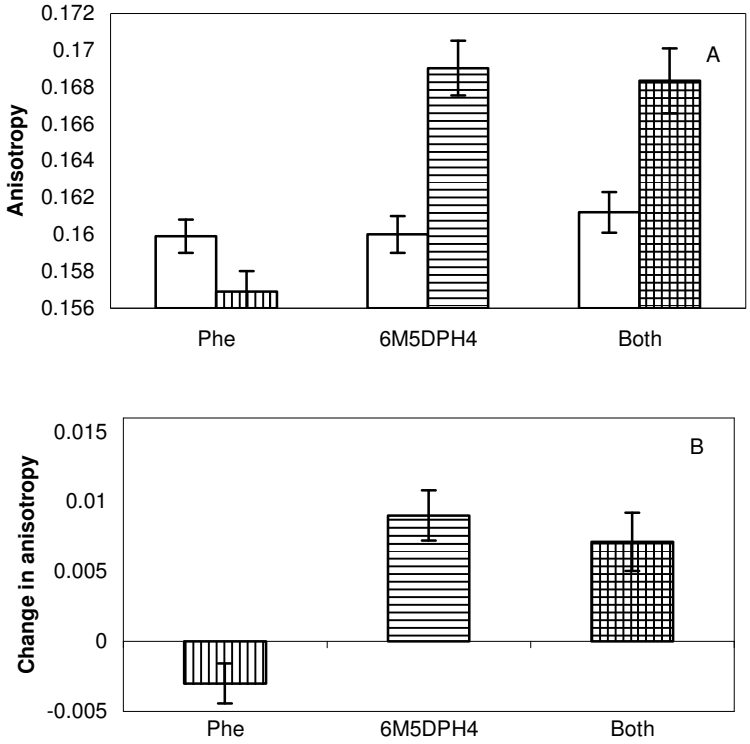


FIGURE 17. Steady-state fluorescence anisotropy of W166F/F184W/W233F/W372F rTyrH (apo) in 25 mM EPPS buffer, pH 7, at 25 ºC: (A) in the absence (empty bars) and presence (filled bars) of 10 mM phenylalanine and 500 μM 6M5DPH$_4$. (B) Change in anisotropy.

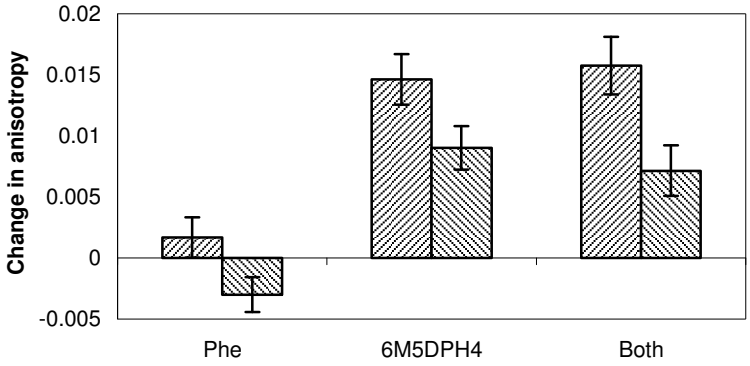


FIGURE 18. Comparison of the change in anisotropy of holo- and apoenzymes. Change in steady-state fluorescence anisotropy of W166F/F184W/W233F/W372F rTyrH (holo-first bar and apo-second bar) in 25 mM EPPS buffer, pH 7, with 10 mM phenylalanine and 500 μM 6M5DPH$_4$.

*Frequency-domain lifetime measurements.* According to Perrin's equation 4, a change in anisotropy could occur because of a change in the fluorescence lifetime and/or the rotational correlation time of the fluorophore. The frequency-domain method was used to characterize the changes in the characteristics of fluorescence emission as a function of the frequency of the modulated excitation. The emission polarizer was oriented at the magic angle to obtain a measured intensity proportional to the total intensity. The two observable characteristics of frequency domain data are phase shift and modulation. The phase shift and modulation of the samples at each frequency of excitation with reference to a known lifetime were obtained in the presence and absence of ligands (Figure 19). To obtain lifetimes, the data were fit to a Gaussian distribution of lifetime (τ) using equation 11, where C is the central lifetime and W is the width. The numerical results are summarized in Table 7. The lifetimes, around 4.1 to 4.4 ns change very little upon binding of the ligands. Therefore, the change in steady state anisotropy upon 6M5DPH$_4$ binding is due to a change in the rotational characteristics of the sole tryptophan.

$$f(\tau) = e^{-(\tau - C)^2 / 2W^2} \Big/ W\sqrt{2\pi} \qquad (11)$$

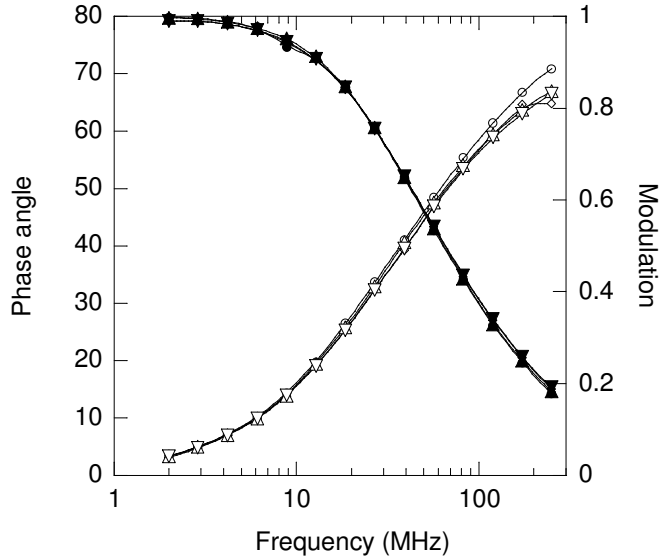


FIGURE 19. Phase shift (open) and modulation ratio (filled) with frequency for enzyme W166F/F184W/W233F/W372F rTyrH alone (circle), with phenylalanine (diamond), with 6M5DPH$_4$ (triangle) and with both (inverted triangle). The lines represent the best fit of the data to a model describing a Gaussian distribution of lifetimes (equation 11).

**Table 7. Fluorescence Lifetimes of the Tryptophan in W166F/F184W/W233F/ W372F rTyrH.**

| Ligands | C (ns) | W (ns) |
|---|---|---|
| No ligand | 4.47 ± 0.04 | 2.53 ± 0.06 |
| 10 mM Phe | 4.24 ± 0.04 | 2.81 ± 0.06 |
| 500 µM 6M5DPH$_4$ | 4.38 ± 0.04 | 2.90 ± 0.06 |
| 500 µM 6M5DPH$_4$ + 10 mM Phe | 4.13 ± 0.05 | 3.01 ± 0.07 |

Data were fit to equation 11.

*Frequency-domain anisotropy measurement.* The different modes of rotation associated with a fluorescent moiety that is amplitude and rates of rotation can be identified and quantified by dynamic anisotropy or differential polarization; this is not possible with steady-state anisotropy measurements. Vertically polarized sinusoidally-

modulated light was used to get differential phase that is difference between perpendicular and parallel phase component of emission and to get modulation ratio that is ratio of the parallel to perpendicular modulation component of emission from W166F/F184W/W233F/W372F rTyrH in the absence and presence of ligands (Figure 20). The presence of a rapid motion is evident from the phase-angle distributions at the higher frequencies. A decreased amplitude of the rapid motion was observed in the presence of 6M5DPH$_4$ while the presence of phenylalanine did not change the amplitude. The curves in Figure 20 represent the best fit of each data set to a model describing a hindered local motion plus a global rotation (equation 9) (*116, 117*). Hindered means the angular range of rotational motion is limited for the tryptophan and the anisotropy ($r_\infty$) does not decay to zero. $r_0$ is anisotropy at time zero and is independent of the rotational motion, $\theta_1$ and $\theta_2$ are the rotational correlation times associated with the two modes of rotation with $\theta_1 << \theta_2$, and $r_\infty$ is the anisotropy that persists for a longer time relative to the short rotational correlation time, $\theta_1$. Consequently, changes in the amplitude of local rotation are reflected as changes in $r_\infty$. When the data are analyzed independently, $\theta_1$ and $\theta_2$ changed very little. Lifetimes for data analysis were fixed with the values in Table 8 even though they were not significantly different. Using all of the data sets in the presence and absence of ligands, a Global analysis was performed in which $\theta_1$ and $\theta_2$ as well as $r_0$ were linked. The values obtained for $\theta_1$, $\theta_2$ and $r_0$ were found to be equal to 1.89 ± 0.25 ns, 115 ± 10 ns, and 0.22 ± 0.03, respectively. The preexponential amplitude of the local component ($r_0$-$r_\infty$) was found to be 6M5DPH$_4$ dependent. This data analysis of binding gave a 50% decrease in the preexponential amplitude in the case of 6M5DPH$_4$ irrespective of phenylalanine (Table 8). With phenylalanine, the preexponential amplitude did not change from the enzyme alone. The calculated cone angle using the equation 10 is decreased by 1 degree in the presence of phenylalanine whereas the cone angle decreases about 5-6 degrees in the presence of 6M5DPH$_4$, irrespective of whether phenylalanine is present (Table 8).

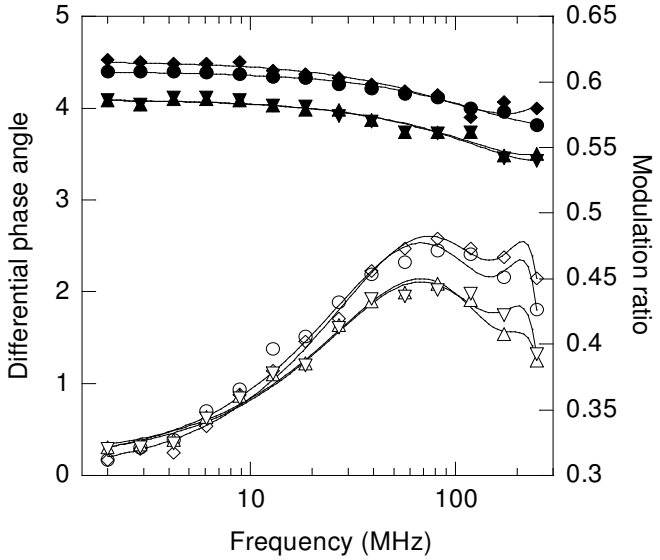


FIGURE 20. Frequency dependence of the differential phase (open) and modulation ratio (filled) of the tryptophan fluorescence of W166F/F184W/W233F/W372F rTyrH, for enzyme alone (circle), phenylalanine (diamond), 6M5DPH4 (triangle) and both (inverted triangle). The curves represent the best fit of the data to a model describing a hindered local motion plus a global rotation (equation 9).

**Table 8. Preexponential Amplitude and Cone Angle of Tryptophan.**

| Ligands | $(r_0-r_\infty)$ | Φ (deg) |
|---|---|---|
| No ligand | 0.048 ± 0.014 | 24 ± 3 |
| 10 mM Phe | 0.041 ± 0.015 | 22 ± 2 |
| 500 μM $6M5DPH_4$ | 0.027 ± 0.014 | 17 ± 2 |
| 500 μM $6M5DPH_4$ + 10 mM Phe | 0.028 ± 0.015 | 18 ± 2 |

Data from differential polarization were fit to a model describing a hindered rotation with a slow global rotation equation 9. The cone angle (Φ) of local rotation for the tryptophan was obtained from equation 10. Here, $(r_0-r_\infty)$ is the preexponential amplitude for the fast rotation.

**DISCUSSION**

The large conformational change in residues 132-148 of PheH when an amino acid substrate is bound (*22*) suggested that this movement is the conformational change required prior to chemistry in these enzymes. Fluorescence anisotropy can provide a sensitive probe of the dynamics of local regions of proteins if they contain a suitable fluorophore. For this study tryptophan was chosen as the fluorophore, since it is a natural component of proteins. To generate a suitable protein for analysis of the loop movement, it was necessary to introduce a tryptophan into the loop and remove the three native tryptophans. The similar kinetic characteristics of these mutant enzymes establishes that the four amino acid changes did not have a significant effect on catalysis of binding, beyond a small change in the $K_m$ value for the tetrahydropterin. Critically, the introduction of the larger tryptophan side chain in place of Phe184 was not problematic. The results described in this chapter establish that this mutant protein is suitable for study of the effects of ligands on the mobility of the active site loop.

The steady-state fluorescence intensity of W166F/F184W/W233F/W372F rTyrH (FeIII) was unaffected by the binding of the ligands used here. This eliminates concerns that the changes in anisotropy are complicated by changes in intensity. It also rules out the use of fluorescence intensity measurements to analyze ligand binding in TyrH. The lack of a change in intensity suggests that the side chain of the tryptophan still has significant solvent exposure when both the amino acid and the pterin are bound. This is consistent with a modeling analysis of the effects of replacing Tyr138 in PheH with tryptophan, which showed that the edge of the indole ring would still be solvent exposed (results not shown).

In contrast to the steady-state fluorescence, fluorescence anisotropy did detect conformational changes upon biding of ligands. In the case of phenylalanine, there was a very small change in the anisotropy within minutes of the addition of a saturating amount of phenylalanine. A larger change was seen during the titration, but this experiment required several hours. Apparently there is a very slow conformational change in the presence of phenylalanine; however, it is much too slow to be relevant to

catalysis. In contrast to the situation with the amino acid ligand, the change in anisotropy upon 6M5DPH$_4$ binding was immediate. In addition, the change was not time-dependent, in that the magnitude of the change in the anisotropy was the same whether 500 μM 6M5DPH$_4$ was added directly or during a slow titration. Consequently, this change can be considered relevant to catalysis. The magnitude of the anisotropy change seen in the presence of the pterin was much greater than that produced by phenylalanine. Moreover, the magnitude of the change with 6M5DPH$_4$ was the same in the presence of phenylalanine. This indicates that 6M5DPH$_4$ alone can decrease the loop mobility in TyrH. Further, the lack of a significant change in the lifetimes of the tryptophan fluorescence in the presence of ligands supports the conclusion that the increase in anisotropy by 6M5DPH$_4$ is due to a decrease in the loop mobility.

Iron at the active site of TyrH plays an important role in binding of ligands. The average anisotropy associated with the apoenzyme is less than that of the holoenzyme indicating that the protein is more flexible in the absence of iron. Even in the absence of iron in the active site, 6M5DPH$_4$ decreased the mobility of the loop, suggesting that the loop movement upon pterin binding is not directly linked to the metal atom. In contrast to the results with the apoenzyme, the presence of the amino acid does affect the magnitude of the anisotropy change seen with the pterin. Thus the effects of binding the amino acid depend upon the presence of iron in the active site. While the structural basis for this is not clear, it does suggest that binding of the amino acid substrate is linked to changes in the iron site.

The dynamic anisotropy experiments clearly confirmed that the presence of 6M5DPH$_4$ changes the environment and the dynamics of the tryptophan moiety in the loop. The rotational correlation time associated with the fast local motion of the loop was not changed in the presence of ligands. This was also the case with the correlation time associated with the global motion of the protein, but this would not be expected to be altered by the small increase in mass upon ligand binding unless there were very large changes in the overall protein conformation. In contrast, if binding of ligands were to eliminate a motion of the loop, there should be a large change in the corresponding

correlation time. Instead, there was a decrease in amplitude of the rotation associated with tryptophan in the loop upon binding of 6M5DPH$_4$. This indicates that the extent of motion of the loop is reduced rather that the rate constant for the motion. The magnitude of this decrease could be modeled as a decrease in the cone angle of the local tryptophan side chain of about 5-6 degrees. Again, this only occurs in the presence of 6M5DPH$_4$, irrespective of the presence of phenylalanine.

Taken together, all of the fluorescence anisotropy experiment suggests that pterin binding alone is responsible for a conformational change in the active site loop. This is in contrast to the crystal structures of PheH which suggests that it is the binding of the amino acid to the binary tetrahydropterin-enzyme complex which causes the conformational change. However, the present results are consistent with both the steady-sate kinetic mechanism of TyrH and the effects of alanine scanning mutagenesis of loop residues. The steady-state kinetic mechanism of TyrH is ordered, with the tetrahydropterin binding before the amino acid (*52*). One explanation for such ordered kinetics is that the binding of the first substrate causes a conformational change necessary for proper formation of the binding site for the subsequent ligand. This model is fully consistent with the results presented here, in that fluorescence anisotropy measurements of the active site loop directly detects a conformational change in the loop upon binding pterin but not amino acid. The results of alanine-scanning mutagenesis were also interpreted as supporting a model in which pterin binding causes a change in the conformation of the loop which is required for proper binding of the amino acid substrate (*119*). Thus, while the results presented here may not be those anticipated from the PheH structures, they are fully consistent with solution studies of TyrH.

In conclusion, the mutant form of TyrH containing a single tryptophan residue in the proposed mobile loop over the active site has proved to be a useful probe of structural changes upon binding of ligands. Binding of a pterin reduces the amplitude of the loop movement and makes a tight binding pocket for the amino acid. The results indicate that the overall decrease in loop mobility is due to 6M5DPH$_4$ binding alone.

# CHAPTER IV

# TYROSINE HYDROXYLASE DYNAMICS PROBED BY H/D EXCHANGE AND MASS SPECTROMETRY

## INTRODUCTION

According to the PheH ternary structure, a large conformational change occurs in residues 131-155 upon amino acid binding to the $BH_4$ complex. The fluorescence anisotropy experiments with mutant TyrH (FeIII) in chapter III suggest that this loop becomes less mobile upon binding of a pterin only. The functional iron in TyrH during catalysis is FeII (scheme 4). The known physiological reductant for iron to make FeIII to FeII is tetrahydrobiopterin ((*80*) in press 2006) (*79*). To understand the dynamics of wild type TyrH under physiological conditions an alternative method has been employed in which its natural substrates and also the FeII and FeIII states of TyrH can be investigated. This chapter will focus on the role of substrates on the conformational change of the loop in TyrH (FeIII) and TyrH (FeII), using H/D exchange mass spectrometry.

H/D exchange mass spectrometry is a sensitive tool to understand conformational changes using exchange of protons on amide nitrogens with deuterium in $D_2O$. The increase in the mass of the region due to deuteriums can be investigated by mass spectrometry of the fragmented protein. Probing hydrogen bonding and structural dynamics in proteins with hydrogen exchange was initiated by Lingerstrom-Lang nearly 50 years ago (*120*). In recent years, the approach of H-D exchange coupled with NMR analysis has revealed detailed site-specific information on bond formation and changes in bond energetics as a function of folding, conformational change, or ligand binding. However, these methods are confined to a small (yet growing) subset of proteins that are amenable to NMR and crystallization analysis. Insights into larger protein systems are facilitated by region specific H-D exchange followed by proteolytic fragmentation and subsequent analysis by mass spectrometric techniques (*121*).

## EXPERIMENTAL PROCEDURES

*Materials.* $6MePH_4$ and $BH_4$ was purchased from B. Schirks Laboratories. L-Phenylalanine and L-tyrosine were purchased from Sigma Chemical Company. Protein & Peptide C18 218TP5215 was purchased from Vydac (Columbia, MI). $6M5DPH_4$ was synthesized according to Moad et al. (*109*) by Dr. Vijay Gawandi from TAMU. Pepsin A from porcine stomach was purchased form Worthington Biochemical Corporation. Methylamine hexamethylene methylamine NONOate was purchased from Cayman Chemicals.

*Protein expression and purification.* rTyrH was expressed in *E. coli* BL21 Star (DE3) cells as previously described with the modifications described in chaper III (*76*). Purified enzyme was stored in 5 mM HEPES, pH 7.0, 100 mM KCl, 10% glycerol at -80 ˚C.

*Identification of peptic fragments of rTyrH.* For sequencing of TyrH peptic fragments, HPLC-MS/MS analysis was performed using a LCQ DECA XP ion-trap mass spectrometer equipped with an electrospray ionization (ESI) source. Forty µg of rTyrH in 5 µl of 5 mM HEPES, pH 7.0, 100 mM KCl and 10% glycerol was diluted to 100 µl with water at 25 °C. 20 µl of this was then mixed with 20 µl of 100 mM sodium citrate, pH 2.4, at 0 °C. An equal weight of pepsin (7.6 µg in 2.5 µl water) was added and the sample was left on ice for 5 minutes. The digested sample of 20 µl was then injected onto a reverse-phase HPLC column (2.1 mm X 150 mm) connected to a ThermoFinnigan Surveyor HPLC (San Jose CA). The buffers used were A) water with ~0.1% formic acid, pH 2.4, and B) 100% acetonitrile with ~0.1% formic acid, pH 2.4. The column was washed with 2% of buffer B for 5 min by direct flow at a rate of 200 µl/min. Peptides were separated by using a gradient of 20%-60% buffer B over 15 min at 200 µl/min. The HPLC injection loop, all buffers and the column were immersed in an ice bath to mimic the H/D experiments. The mass spectrometer was set to detect the total intensity of the ions in the *m/z* range of 400-2000. Mass scanning was followed by collision-induced dissociation in positive mode to acquire a MS/MS spectrum on the most intense ion within a peak during the LC run. Angiotensin was used to optimize the

sheath, auxillary nitrogen gas pressures and tube lens voltage. The headed capillary was maintained at 150 °C, and spray voltage was kept at 3.0 kV. The detector was calibrated to unit resolution and the data were collected at a scan time of 1 second and a peak width of 0.5 by scanning 400-2000 *m/z*. The MS/MS spectra were interpreted with TurboSEQUEST software, a search tool from BioWorks (Thermo Finningan, Version 3.1). TurboSEQUEST creates an experimental file of peptide masses (*.dta* files) from MS/MS experiments (*.raw* files) and correlates this with theoretical mass spectra produced from sequences generated from a protein fasta database. The identities of the peptides from the experimental file were further confirmed from a peptic peptide map of TyrH generated with the program MS-digest by Peter Baker Instructions (http://prospector.ucsf.edu /ucsfhtml4.0/msdigest.htm).

*H/D exchange studies.* HPLC/ESI-MS was used to determine the extent of deuterium incorporation into rTyrH (*122*). H/D exchange from solvent was initiated by dilution of 120 µg rTyrH in 15 µl of 5 mM HEPES, pH 7.0, 100 mM KCl, 10% glycerol into 300 µl of $D_2O$ (20 volumes) at 25 ºC. Stock solutions of 5.25 mM $6MePH_4$ and 1.05 mM $BH_4$ were made in anaerobic $D_2O$ to prevent autooxidation. For reactions under anaerobic conditions, the solution containing enzyme and the solution containing the ligands were made anaerobic by alternately exposing to argon and vacuum. The ligand solution was then added to the enzyme solution with a syringe flushed with argon gas. In case of making complex of TyrH with FeII, equimolar concentrations of anaerobic ferrous ammonium sulfate was added to anaerobic apoenzyme and incubated on ice for 10 min. In the case of nitric oxide, methylamine hexamethylene methylamine NONOate was dissolved in anaerobic $D_2O$ and exposed for a very short time to argon and vacuum to remove any oxygen before being mixed with the enzyme; after 2 min, tyrosine and $BH_4$ were added to the enzyme-NO complex. At the indicated time intervals, a 20 µl sample was removed from the solution and mixed with an equal volume of 100 mM sodium citrate buffer, pH 2.4, at 0 ºC. Immediately, 2.5 µl pepsin in water (3.1 µg/µl) was added, and the sample was digested at 0 ºC for 5 min and then injected onto the HPLC column. HPLC conditions were the same as above. The buffers, loop and column

were immersed in an ice bath to minimize D/H exchange with HPLC solvents during chromatography. LC-MS analysis of the HPLC effluent was done to determine the extent of deuterium incorporation into rTyrH.

*Calculation of the deuterium labeling distribution.* The isotope pattern of the loop fragment formed by a mixture of ions with different amounts of deuterium was identified from the total ion chromatograph using Qual Browser software. MagTran 1.0 beta 9 software (*123*) was used to determine the centroid of the extracted composite isotope envelope. The number of amide hydrogens exchanged at a given time was determined by fitting the data to equation 12 using KaleidaGraph (Synergy software). Here, D is the number of deuterium atoms present in a peptide, N is the number of peptide amide linkages in a segment, and $k_i$ is the hydrogen-deuterium exchange rate constant for each peptide linkage.

$$D = N - \sum_{i=1}^{N} e^{-k_i t} \qquad (12)$$

*General principle of H/D exchange mass spectrometry.* Hydrogen-deuterium (H/D) exchange is a popular and sensitive method for elucidation of protein structural changes. Phenomenologically, the method is based on the H/D exchange of amide protons located at the peptide backbone participating in intramolecular hydrogen bonding because these are the slowest to exchange and thus the most easily detected by experiments. The method was introduced by Linderstrom-Lang to study protein dynamics (*120*). In 1993, Zhang and Smith were the first to combine H/D exchange with mass spectrometry to improve the spatial resolution by proteolysis and mass analysis of the peptide fragments (*124*). Since then H/D exchange has emerged as an essential tool to study protein structure in solution. From this method one can obtain information on protein-protein and protein-ligand interactions and on conformational changes in protein with a resolution of 1-10 residues (*120*). The advantages of this technique are the lack of size limitation to the protein, working protein concentrations in the sub-micromolar range, and its applicability to membrane proteins (*124*).

Theoretically, the exchange of an amide hydrogen is a chemical exchange with solvent where base catalyses the proton abstraction at neutral pH (*125*). The intrinsic rate of exchange of an exposed proton is on the order of 10 $s^{-1}$. The exchange rate decreases by as much as eight orders of magnitudes when the hydrogen participates in an intramolecular hydrogen bond. The rates of H/D exchange in a folded protein depend on structural fluctuations that result in open and closed conformations (*126*). According to such a model, exchange–labile hydrogen that is slow to exchange most often resides in the closed state, from which exchange cannot occur. Occasionally the protein experiences a motion that brings the amide hydrogen to an open state from which exchange can occur. The opening motion proceeds with the rate constant $k_o$ and the closing motion with the rate constant $k_c$. Exchange can occur with the rate constant $k_i$ from the open form. The observed rate constant $k_{ex}$ from such a model is given by equation 11.

$$NH_{cl} \underset{k_c}{\overset{k_o}{\rightleftharpoons}} NH_{op} \xrightarrow{k_i} ND$$

$$k_{ex} = k_i k_o / (k_i + k_c) \qquad (11)$$

Once an amide hydrogen reaches the open state, the balance between closing without exchange and moving forward with exchange dictates the two limits EX1 and EX2. In the EX2 limit of hydrogen exchange, $k_c >> k_i$, and the equation simplifies to $k_{ex} = (k_o / k_c)k_i = K_{eq}k_i$. Here, $k_o/k_c$ is equivalent to the equilibrium constant for opening, $K_{eq}$. In most studies, $k_i$ depends on the hydroxide ion concentration, so $k_{ex}$ represents an apparent bimolecular. Since $k_i$ can be calculated from model compound data, exchange rates from the EX2 limit can be used to determine $K_{eq}$ if the model is correct. In the EX1 limit of hydrogen exchange, $k_i >> k_c$ and equation 11 simplifies to $k_{ex} = k_o$; exchange always occurs from the open state before the amide proton closes to exchange. The two mechanisms can be distinguished by the the isotopic pattern of the deuterium exchanged fragment seen in the mass spectrometer (Figure 20) (*122*). H/D exchange via an EX2 mechanism increases the mass of peptide and shows a binomial distribution of peaks

(Figure 21). An increase in mass due to deuteriums can be calculated from the centroid of mass. From the time course of exchange of deuteriums, one can determine the rate constants for exchange using equation 12.

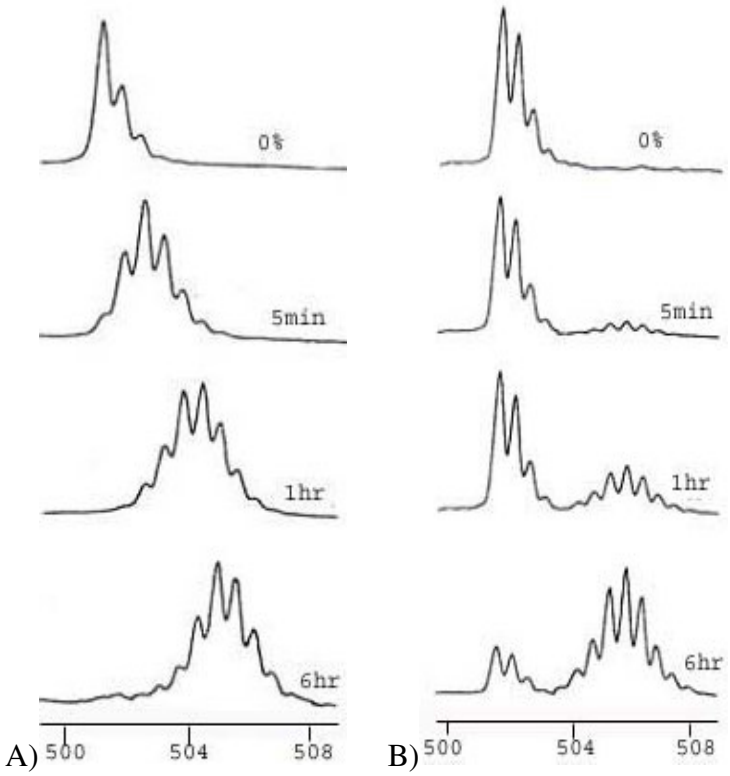


FIGURE 21. Isotopic patterns of deuterium atom exchanged fragments: A) EX2 mechanism and B) EX1 mechanism (*122*).

**RESULTS**

*Identification of peptic fragments.* Prior to H/D exchange experiments, TyrH peptic peptides were sequenced by HPLC/ESI-MS/MS. Pepsin-digested TyrH was separated on HPLC and the eluted fragments were sequenced on a mass spectrometer as described in Experimental Procedures. The sequence of peptide fragments in each scan (Table 9) was identified by TurboSEQUEST software, a search tool from BioWorks (Thermo Finningan, Version 3.1). The identities of the peptic peptides from the experiment were further confirmed from a peptic peptide map of TyrH generated with

MS-digest program by Peter Baker Instructions (http://prospector.ucsf.edu /ucsfhtml4.0/msdigest.htm). From this 71% of the TyrH sequence (Table 9) was obtained from single run and 72% of the sequence was identified from different runs (Figure 22). The pepsin digested TyrH fragments were found to be highly reproducible under the final optimized conditions.

**Table 9. Sequence of Peptic Peptides of TyrH.**

| Scan(s) | Sequence | MH+ | Charge |
|---|---|---|---|
| 568 - 574 | L.ASLGASDEE.I | 878.37 | 1 |
| 572 - 577 | L.KGLYATHACREHLEG.F | 1684.82 | 3 |
| 584 - 588 | Q.YIRHASSPMHSPEPDCC.H | 1929.80 | 3 |
| 589 | Q.YIRHASSPMHSPEPDCC.H | 1929.80 | 2 |
| 610 - 614 | F.EAKIHHLETRPAQRPLAGSPHLEY.F | 2750.45 | 3 |
| 640 - 644 | L.HTLAHALSAIS.- | 1120.61 | 2 |
| 661 | L.LERYCGY.R | 903.40 | 2 |
| 664 - 669 | F.SQDIGL.A | 632.33 | 1 |
| 668 - 672 | L.FSLRGTKPSSL.S | 1192.67 | 2 |
| 673 - 677 | A.FQYKHGEPIPHVEY.T | 1743.85 | 3 |
| 676 - 684 | Y.VTLKGLYATHACREHLEG.F | 1998.02 | 3 |
| 714 - 716 | L.LSSYGEL.L | 768.38 | 1 |
| 725 | Y.GELLHSLSEE.P | 1113.54 | 2 |
| 736 - 741 | E.IAFQYKHGEPIPHVEYTAEE.I | 2358.14 | 3 |
| 742 | E.IAFQYKHGEPIPHVEYTAE.E | 2229.10 | 3 |
| 748 - 752 | A.FRVFQCTQ.Y | 1028.50 | 2 |
| 760 - 764 | A.DRTFAQF.S | 884.43 | 2 |
| 762 | L.LHSLSEEPEVRAFDPDTA.A | 2012.96 | 3 |
| 765 - 768 | A.VVFEERDGNAVL.N | 1347.69 | 2 |
| 769 - 772 | E.IAFQYKHGEPIPHVEY.T | 1927.97 | 3 |
| 773 - 778 | E.FGLCKQNGEL.K | 1108.55 | 2 |
| 776 | A.IDVLDSPHTIQRSLE.G | 1722.90 | 2 |
| 781 | E.IATWKEVY.V | 1009.54 | 2 |
| 785 | A.IDVLDSPHTIQRSLE.G | 1722.90 | 3 |
| 793 | L.ADRTFAQF.S | 955.46 | 2 |
| 798 - 801 | L.SRAVKVFETF.E | 1183.65 | 2 |
| 800 - 804 | F.LKERTGFQLRPVAGL.L | 1684.99 | 3 |
| 817 - 820 | L.IEDARKEREAAAAAAAAAVASSEPGNPLEA.V | 2936.47 | 3 |
| 821 - 824 | F.VRFEVPSGDL.A | 1118.58 | 2 |
| 825 - 830 | L.DKCHHLVTKFDPDLDL.D | 1895.93 | 3 |
| 825 - 830 | E.LDKCHHLVTKFDPDLD.L | 1895.93 | 3 |
| 826 - 828 | C.HELLGHVPMLA.D | 1216.65 | 2 |

**Table 9. Continued.**

| Scan(s) | Sequence | MH+ | Charge |
|---|---|---|---|
| 829 - 832 | E.LDKCHHLVTKFDPDLDL.D | 2009.02 | 3 |
| 836 | L.DKCHHLVTKFDPDLDL.D | 1895.93 | 2 |
| 840 - 844 | E.FGLCKQNGELKAYGAGL.L | 1768.91 | 3 |
| 852 | F.QLRPVAGLL.S | 966.61 | 2 |
| 868 - 872 | C.HELLGHVPML.A | 1145.61 | 2 |
| 870 - 873 | L.LSARDFL.A | 821.45 | 2 |
| 888 - 892 | Y.FVRFEVPSGDL.A | 1265.65 | 2 |
| 890 | S.LAFRVFQCTQ.Y | 1212.62 | 2 |
| 893 - 896 | F.LKERTGFQLRPVAGLL.S | 1798.07 | 3 |
| 894 | E.FGLCKQNGELKAYGAGLLSS.Y | 2056.05 | 3 |
| 905 - 908 | T.WKEVYVTL.K | 1037.57 | 2 |
| 906 | L.EDVSRFLKERTGFQLRPVAGL.L | 2418.33 | 3 |
| 925 | L.KAYGAGLLSSYGEL.L | 1428.74 | 2 |
| 928 - 932 | A.IDVLDSPHTIQRSLEGVQDEL.H | 2364.20 | 3 |
| 929 - 933 | A.IDVLDSPHTIQRSLEGVQDEL.H | 2364.20 | 2 |
| 942 | L.AIDVLDSPHTIQRSLEGVQDEL.H | 2435.24 | 2 |
| 944 | L.AIDVLDSPHTIQRSLEGVQDEL.H | 2435.24 | 3 |
| 948 - 952 | E.PEVRAFDPDTAAVQPYQDQTYQPVYF.V | 3045.43 | 2 |
| 960 | E.IATWKEVYVTL.K | 1322.74 | 2 |
| 965 - 985 | E.FGLCKQNGELKAYGAGLLSSYGEL.L | 2518.27 | 3 |
| 969 | L.LSSYGELLHSLSEE.P | 1563.75 | 2 |
| 984 | Q.DELHTLAHALSAIS. | 1477.77 | 2 |

Periods indicates the pepsin sites.

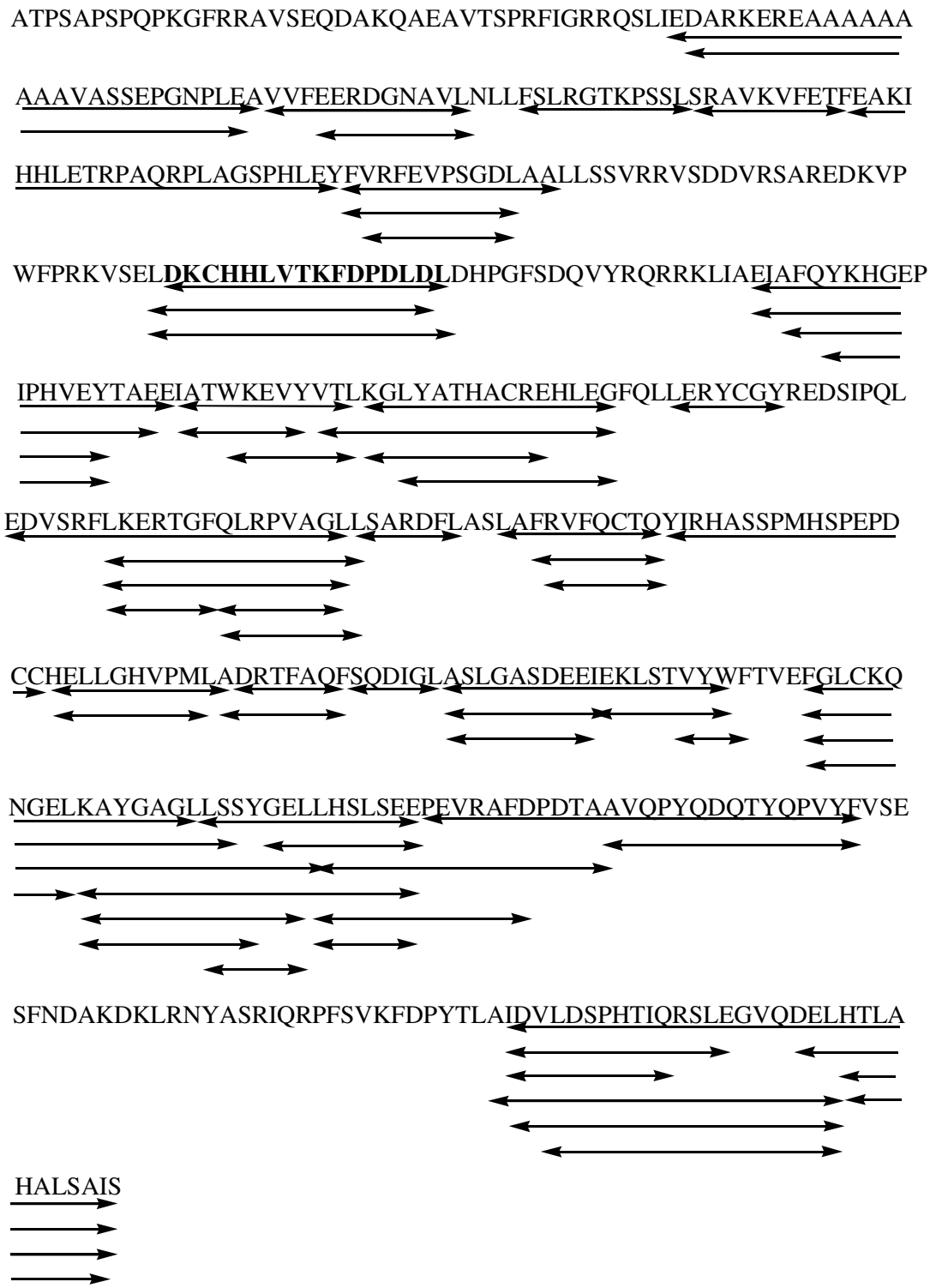


FIGURE 22. TyrH peptic peptide map. The arrows indicate the individual peptides observed from MS/MS. Loop residues are shown in bold.

*H/D exchange studies and time dependent deuterium incorporation.* The previous analysis of W166F/F184W/W233F/W372F TyrH by fluorescence anisotropy spectroscopy indicated that the loop (residues 177-200) is less mobile in the presence of substrates. The structural changes of TyrH on substrate binding were further probed with H/D exchange. It was initiated by dilution of rTyrH into 20 volumes of $D_2O$. The extent of deuteration of the loop peptide was followed as a function of time at pH 7.0. At regular intervals samples were collected, quenched and digested with pepsin. The peptic peptide fragments were separated by HPLC and the fragments were directly sent to a mass spectrometer as described in Experimental Procedures. The loop fragment having residues 174-189 (DKCHHLVTKFDPDLDL) with mass 1895.93 and charge +3 (Table 9) were analyzed for deuterium incorporation. This loop fragment with M/Z value of 632.6 was identified from the total ion chromatograph (Figure 23A). The isotopically labeled peptide with M/Z value 632.6 was eluted around the same time in all the experiments. For each run, the binomial envelope formed due to deuterium incorporation onto the loop fragment (Figure 23B) was exported to MagTran, a software to identify the increase in mass.

(A)

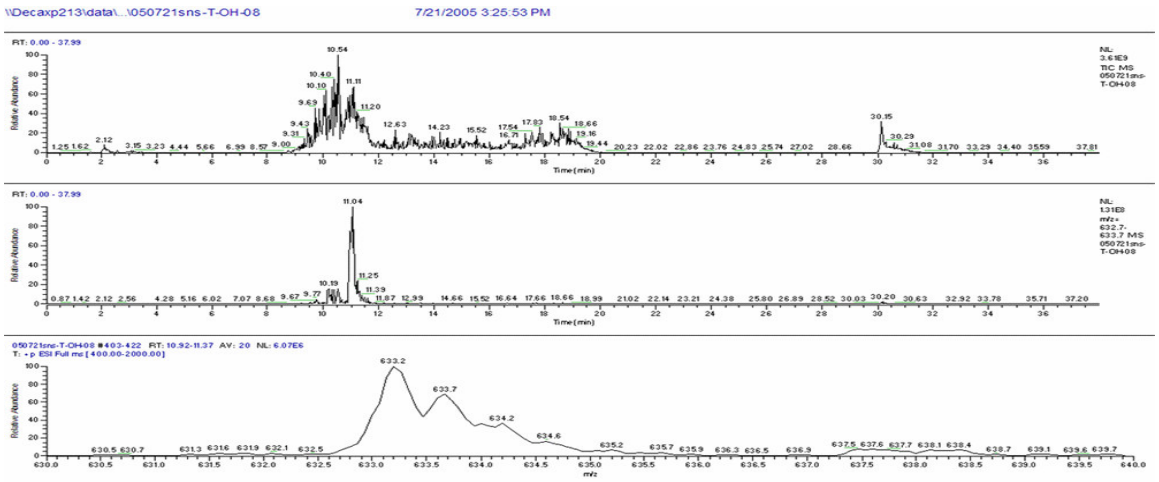


(B)

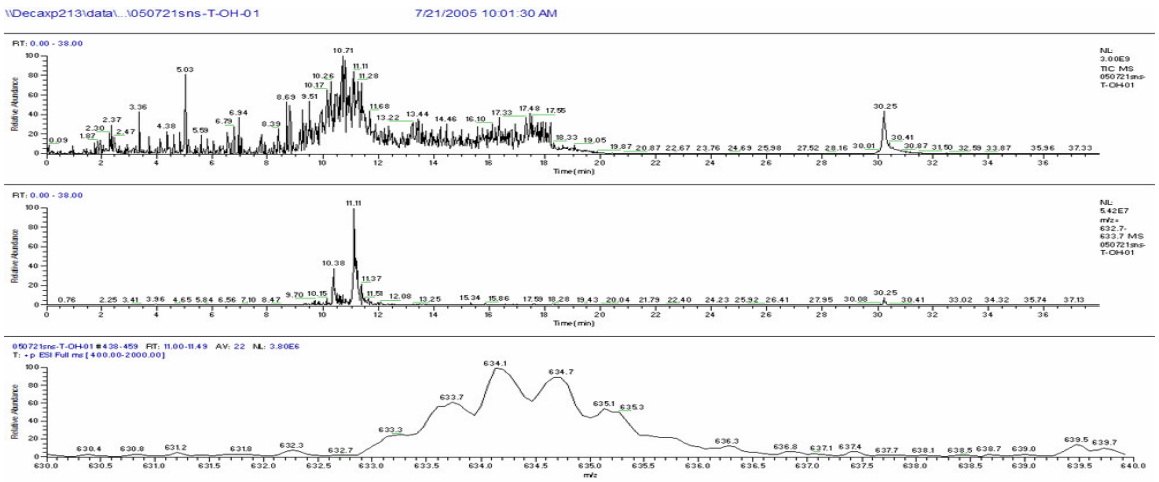


FIGURE 23. Characteristics of the loop fragment in A) $H_2O$ and B) $D_2O$. The top panel is the total ion chromatograph of TyrH peptic peptides from MS-ESI, the loop fragment elution time in the middle panel and the lower panel is the enlarged region of the middle panel between 630.0 and 640.0 M/Z values.

With time, an increase in the mass of the loop fragment was observed. The number of deuteriums on the loop was calculated. The kinetics of deuterium exchange in the presence and absence of ligands were analyzed. Figures 24, 25 and 26 are representative of the results obtained showing the number of deuteriums trapped onto the loop in the presence of ligands. The data were fit to equation 12 where D is the number

of deuterium atoms present in a peptide, N is the number of peptide amide linkages in a segment, and $k_i$ is the hydrogen-deuterium exchange rate constant for each peptide linkage. Over the time course of exchange experiments, the increase in the mass of the loop was biphasic (Figure 24, 25 and 25; and Table 10) in all cases. The number of deuteriums at equilibrium was found to be between 5.7 ± 0.7 and 9.3 ± 0.6. Fast exchange rates of deuteriums were observed between 0.9 ± 0.01 to 2.25 ± 0.54 per min. Significant changes in slow deuterium exchange rates were observed for FeIII vs FeII. Where the rates were less than 0.005 ± 0.002 per min for TyrH (FeIII) and for TyrH (FeII) rates were 0.010 ± 0,003 to 0.022 ± 0.004 per min in the presence of ligands. The exchange kinetics of loop did not change in the presence of tyrosine. Whatever the changes observed were due to pterin binding.

The time course of dependent H/D of exchange of loop in TyrH (FeIII) was done in the presence of tyrosine and $6M5DPH_4$. $6M5DPH_4$ is a pterin analogue. The kinetics of deuterium exchange did not change in the presence of tyrosine whereas $6M5DPH_4$ caused an increase in mass (Figure 24 and Table 10). The exchange rates associated with these deuteriums did not change. The total number of fast exchanging deuterium increased from 4 to 6 in the presence of $6M5DPH_4$.

The time course of dependent H/D of exchange of loop in TyrH (FeII) was done under anaerobic conditions in the presence of tyrosine, $6MePH_4$ and $BH_4$ (Figure 25 and 26). $6MePH_4$ and $BH_4$ reduce the TyrH (FeIII) to TyrH (FeII). The reconstitution of TyrH (FeII) was explained in Experimental Procedures. The kinetics of H/D exchange in the presence of pterin resulted in increase of number of deuteriums on the loop and no further change observed in the presence of tyrosine. In case of tyrosine, $6MePH_4$ and $BH_4$, the slow exchange rates are found to be around 0.011 ± 0.004 per min (Table 10). The rates did not change in the presence of tyrosine for $6MePH_4$ whereas rates were increased two fold for $BH_4$ (Table 10). NO mimics like oxygen. The kinetics of H/D exchange does not change from the $BH_4$ and tyrosine (Figure 26 and Table 10).

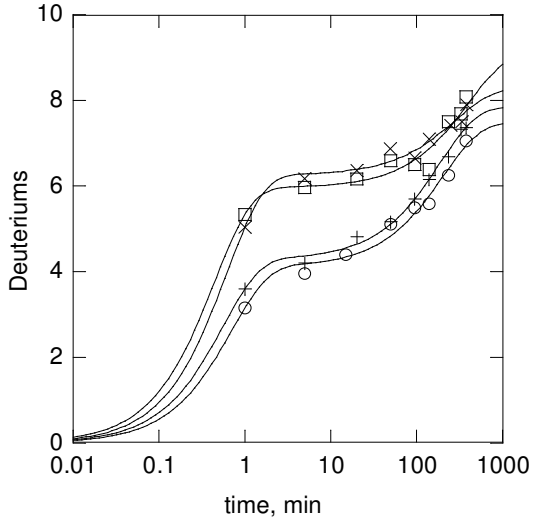


FIGURE 24. Effects of ligands on the kinetics of deuterium incorporation into residues 174-189 in TyrH (FeIII). TyrH alone (○), 1 mM tyrosine (+), 5 mM 6M5DPH$_4$ (□), and both 5 mM 6M5DPH$_4$ and 1 mM tyrosine (X). The lines are fits of the data to equation 12.

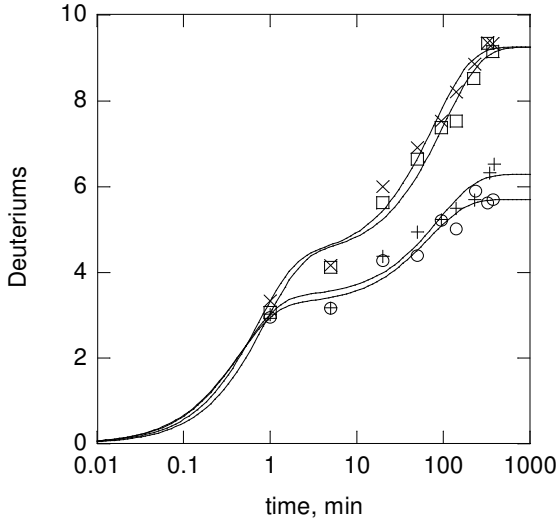


FIGURE 25. Effects of ligands on the kinetics of deuterium incorporation into residues 174-189 in TyrH (FeII) upon ligand binding. TyrH alone (○), 1 mM tyrosine (+), 5 mM 6MePH$_4$ (□), and both 5 mM 6MePH$_4$ and 1 mM tyrosine (X). The lines are fits of the data to equation 12.

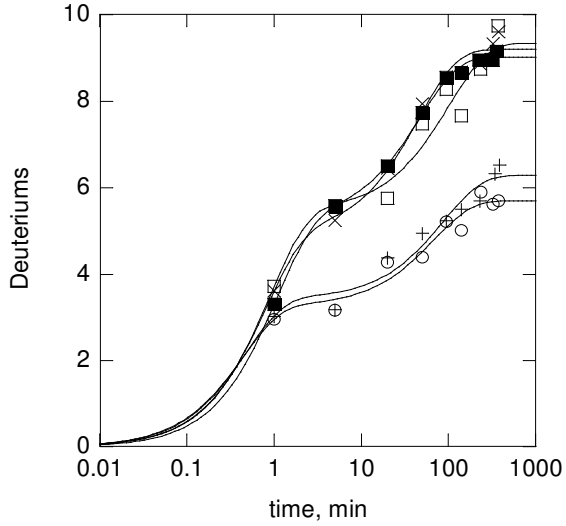


FIGURE 26. Effects of ligands on the kinetics of deuterium incorporation into residues 174-189 in TyrH (FeII) upon ligand binding. TyrH alone (○), 1 mM tyrosine (+), 1 mM $BH_4$ (□), both 1 mM $BH_4$ and 1 mM tyrosine (X), and 1mM $BH_4$, 1 mM tyrosine and equimolar NO (■). The lines are fits of the data to equation 12.

**Table 10. Extent of Deuterium Incorporation and Their Rates.**

| Conditions | Mass at equilibrium | Number of D | $k_1$ ($min^{-1}$) | Number of D | $k_2$ ($min^{-1}$) |
|---|---|---|---|---|---|
| **TyrH (FeIII)** | | | | | |
| No ligands | 7.5 ± 0.7 | 4.1 ± 0.3 | 1.44 ± 0.29 | 3.4 ± 0.6 | 0.005 ± 0.002 |
| Tyr | 7.8 ± 0.3 | 4.3 ± 0.2 | 1.80 ± 0.23 | 3.6 ± 0.3 | 0.005 ± 0.001 |
| $6M5DPH_4$ | 9.1 ± 0.7 | 5.9 ± 0.3 | 2.25 ± 0.54 | 3.1 ± 2.6 | 0.002 ± 0.003 |
| Tyr+$6M5DPH_4$ | 8.3 ± 0.9 | 6.3 ± 0.2 | 1.63 ± 0.19 | 2.1 ± 0.8 | 0.004 ± 0.002 |
| **TyrH (FeII)** | | | | | |
| No ligands | 5.7 ± 0.2 | 3.2 ± 0.4 | 2.29 ± 1.27 | 2.5 ±0.3 | 0.015 ± 0.005 |
| Tyr | 6.3 ± 0.3 | 3.4 ± 0.5 | 2.10 ± 1.12 | 2.9 ± 0.4 | 0.011 ± 0.004 |
| $6MePH_4$ | 9.2 ± 0.4 | 4.4 ± 0.6 | 1.15 ± 0.38 | 4.9 ± 0.5 | 0.010 ± 0.003 |
| Tyr+$6MePH_4$ | 9.3 ± 0.3 | 4.3 ± 0.6 | 1.39 ± 0.46 | 4.9 ± 0.4 | 0.013 ± 0.003 |
| $BH_4$ | 9.3 ± 0.6 | 5.4 ± 1.1 | 1.12 ± 0.50 | 3.9 ± 0.8 | 0.010 ± 0.006 |
| Tyr+$BH_4$ | 9.2 ± 0.2 | 4.9 ± 0.5 | 1.26 ± 0.29 | 4.3 ± 0.4 | 0.022 ± 0.004 |
| Tyr+$BH_4$+NO | 9.1 ± 0.1 | 5.2 ± 0.2 | 0.95 ± 0.01 | 3.8 ± 0.1 | 0.021 ± 0.002 |

Conditions: Kinetics traces are illustrated in Figures 24, 25 and 26. The concentrations of ligands are 1 mM tyrosine, 5 mM $6M5DPH_4$, 5mM $6MePH_4$, 1mM $BH_4$, and 143 µM NO.

## DISCUSSION

The crystal structure of the PheH ternary complex shows a large conformational change in residues 131-155 upon binding of an amino acid. In contrast, the fluorescence anisotropy experiments in Chapter III suggested that binding of $6M5DPH_4$, a pterin analogue, to TyrH reduces the movement of the loop in that enzyme, but that binding of the amino acid has little effect on the loop. However, the results from the fluorescence experiments may not be directly relevant to catalysis. $6M5DPH_4$ is an inhibitor rather than a substrate, and the iron was in the inactive ferric form for those experiments. A lesser concern is that phenylalanine was used instead of the physiological substrate tyrosine. To investigate the conformational change in the loop under catalytic conditions,

that is, in the presence of natural substrates and with ferrous enzyme, H/D exchange analyses were employed. A variation of the techniques of Englander et al. (*125*) was used to detect structural changes upon ligand binding.

Qualitatively, the results of the H/D analyses confirm the conclusions drawn from the fluorescence experiments. In the case of ferric TyrH, the H/D exchange kinetics of the loop did not change in the presence of tyrosine. In contrast addition of $6M5DPH_4$, a pterin analogue, increased the number of fast exchangeable deuteriums, indicating that the chemical environment of the loop had changed. The lack of further change observed in the presence of tyrosine indicates that the binding of tyrosine did not change the chemical environment of the loop beyond that produced by $6M5DPH_4$. These results are identical those of the fluorescence analyses.

The H/D experiments could also be done with ferrous enzyme, unlike the fluorescence analyses. Both $6MePH_4$ and $BH_4$ readily reduce TyrH (*79, 80*). As long as the experiments are done under anaerobic condition oxidation of the iron does not occur. The increased deuterium content of the loop in the presence of tetrahydropterin was due to an increase in the number of both the slow and the fast exchanging deuteriums. This is qualitatively comparable to the change produced by $6M5DPH_4$ and the ferric enzyme. However, there was a 2 to 4-fold increase in the rate constant for the slowly exchanging deuteriums, suggesting that there are differences in the conformational changes in the two different experiments and that the changes detected by fluorescence measurements are a subset of the conformational changes which occur during catalysis. There was also a difference in the kinetics of exchange with $6MePH_4$ versus $BH_4$, the physiological substrate. In addition to the differences seen in the presence and absence of the tetrahydropterin, the presence of tyrosine resulted in a two-fold increase in the slow deuterium exchange rates with $BH_4$, in contrast to the lack of an effect with $6MePH_4$. $BH_4$ has a 1,2-dihydroxypropyl group at C6 instead of the methyl group found in $6MePH_4$. The differences in the exchange kinetics between the two tetrahydropterin suggest that interactions with the dihydroxypropyl side chain are linked to the conformational change. While $6MePH_4$ is routinely used as a substrate for TyrH in place

of $BH_4$, there are differences in the kinetics with the two different pterins. For example, there is much greater substrate inhibition with tyrosine when $BH_4$ is used (*52*); indeed, that is one reason that $BH_4$ is avoided.

One difference between the experiments with the tetrahydropterins and with the catalytic reaction is that the latter involves oxygen. Oxygen could not be included with the other substrates, since that would have resulted in turnover. Nitric oxide has been used as an oxygen mimic for a number of iron proteins (*127*). The lack of any change in the exchange kinetics when NO was included suggests that oxygen binding is not linked to a conformational change prior to catalysis.

In conclusion, these results support the conclusions drawn from the fluorescence anisotropy experiments: amino acid binding does not change the mobility of the loop or changes it very little, whereas pterin binding substantially decreases its mobility. These results are also consistent with a kinetic mechanism (*52*) in which tetrahydropterin binds first to establish a binding pocket for the amino acid. However, the results do not identify the critical conformational changes or changes required for initiation of catalysis. Identification of those will require further experiments. These will include analysis of the exchange dynamics of the remainder of the peptic peptides in TyrH and studies with mutant TyrH enzymes, especially F184A.

# CHAPTER V

## SUMMARY

The studies presented here have focused on the role of protein structure on regulation and catalysis in TyrH. In Chapter II, the effect of phosphorylation on the human TyrH isoforms were determined. The four isoforms were cloned and characterized. Phosphorylated and unphosphorylated isoforms were used to study the binding of DOPA and dopamine to understand the regulatory mechanism. The $K_d$ value for DOPA increases two fold for isoform 1 upon phosphorylation and this value decreases as the length of the regulatory domain is increased. Dopamine binds very tightly to all four isoforms, upon phosphorylation $K_d$ value increased about 30 fold. Dopamine was found to be the key regulating catecholamine for hTyrH isoforms rather than DOPA.

Chapters III and IV focused on loop movement using fluorescent anisotropy and H/D exchange LC/MS mass spectroscopy. In TyrH, loop residues 177-200 play an important role in binding of tyrosine and DOPA formation. $6M5DPH_4$ binds to apo and holoenzymes and decreases the loop mobility. Iron seems to play an important role in binding of the phenylalanine. Further characterization of the mobility of the tryptophan in the loop by frequency-domain anisotropy demonstrated a decreased amplitude of the local rotation in the presence of $6M5DPH_4$ alone. The structural changes were further probed with H/D exchange mass spectroscopy. The results confirmed that the change in the chemical environment of the loop is dependent on the pterin which does not change with the presence or absence of tyrosine. The results show the conformational change in the loop is primarily due to pterin binding. The conformational change in the loop produced upon pterin binding allows the amino acid to bind to TyrH and the chemistry to take place. This supports the kinetics of alanine scanning mutations of loop residues in TyrH.

## REFERENCES


1. Kaufman, S., Bridgers, W.F., Eisenberg, F., and Friedman, S. (1962) *Biochem. Biophys. Res. Commun. 9*, 497-502.

2. Udenfriend, S., and Cooper, J.R. (1952) *J. Biol. Chem. 194*, 503-511.

3. Nagatsu, T., Levitt, M., and Udenfriend, S. (1964) *J. Biol. Chem. 239*, 2910-2917.

4. Knappskog, P.M., Flatmark, T., Mallet, J., Ludecke, B., and Bartholome, K. (1995) *Hum. Mol. Genet. 4*, 1209-1212.

5. Ludecke, B., Knappskog, P.M., Clayton, P.T., Surtees, R.A.H., Clelland, J.D., Heales, S.J.R., Brand, M.P., Bartholome, K., and Flatmark, T. (1996) *Hum. Mol. Genet. 5*, 1023-1028.

6. van den Heuvel, L.P.W.J., Luiten, B., Smeitink, J.A.M., deRijk-van Andel, J.F., Hyland, K., Steenbergen-Spanjers, G.C.H., Janssen, R.J.T., and Wevers, R.A. (1998) *Hum. Genet. 102*, 644-646.

7. Roy, A., DeJong, J., and Linnoila, M. (1989) *Arch. Gen. Psychiatry 46*, 609-612.

8. Grahame-Smith, D.G. (1992) in *Serotonin 1A Receptors in Depression and Anxiety* (Stahl, S.M., Ed.) pp 1-21, Raven Press, Ltd., New York.

9. Brunner, H.G., Nelen, M., Breakefield, X.O., Ropers, H.H., and van Oost, B.A. (1993) *Science 262*, 578-580.

10. Nakata, H., and Fujisawa, H. (1982) *Eur. J. Biochem. 124*, 595-601.

11. Okuno, S., and Fujisawa, H. (1982) *Eur. J. Biochem. 122*, 49-55.

12. Kappock, T.J., Harkins, P.C., Friedenberg, S., and Caradonna, J.P. (1995) *J. Biol. Chem. 270*, 30532-30544.

13. Fisher, D.B., and Kaufman, S. (1973) *J. Biol. Chem. 248*, 4345-4353.

14. Daubner, S.C., and Fitzpatrick, P.F. (1993) in *Chemistry and Biology of Pteridines and Folates* (Ayling, J.E., Nair, M.G., & Baugh, C.M., Eds.) pp 87-92, Plenum Press, New York.

15. Ramsey, A.J., and Fitzpatrick, P.F. (1998) *Biochemistry 37*, 8980-8986.

16. Kobe, B., Jennings, I.G., House, C.M., Michell, B.J., Goodwill, K.E., Santarsiero, B.D., Stevens, R.C., Cotton, R.G.H., and Kemp, B.E. (1999) *Nat. Struct. Biol. 6*, 442-448.

17. Goodwill, K.E., Sabatier, C., Marks, C., Raag, R., Fitzpatrick, P.F., and Stevens, R.C. (1997) *Nat. Struct. Biol. 4*, 578-585.

18. Goodwill, K.E., Sabatier, C., and Stevens, R.C. (1998) *Biochemistry 37*, 13437-13445.

19. Fusetti, F., Erlandsen, H., Flatmark, T., and Stevens, R.C. (1998) *J. Biol. Chem. 273*, 16962-16967.

20. Andersen, O.A., Flatmark, T., and Hough, E. (2001) *J. Mol. Biol. 314*, 279-291.

21. Wang, L., Erlandsen, H., Haavik, J., Knappskog, P.M., and Stevens, R.C. (2002) *Biochemistry 41*, 12569-12574.

22. Andersen, O.A., Flatmark, T., and Hough, E. (2002) *J. Mol. Biol. 320*, 1095-1108.

23. Daubner, S.C., Melendez, J., and Fitzpatrick, P.F. (2000) *Biochemistry 39*, 9652-9661.

24. McKinney, J., Teigen, K., Frøystein, N.A., Salaün, C., Knappskog, P.M., Haavik, J., and Martínez, A. (2001) *Biochemistry 40*, 15591-15601.

25. Daubner, S.C. , Moran, G.R., and Fitzpatrick, P.F. (2002) *Biochem. Biophys. Res. Commun. 292*, 639-641.

26. Daubner, S.C., Hillas, P.J., and Fitzpatrick, P.F. (1997) *Biochemistry 36*, 11574-11582.

27. Fitzpatrick, P.F. (1991) *Biochemistry 30*, 6386-6391.

28. Moran, G.R., Daubner, S.C., and Fitzpatrick, P.F. (1998) *J. Biol. Chem. 273*, 12259-12266.

29. Hegg, E.L., and Que, L. (1997) *Eur. J. Biochem. 250*, 625-629.

30. Koshland, D.E. (1958) *Proc. Natl. Acad. Sci. U.S.A.* 98-104.

31. Andersen, M.D., Shaffer, J., and Adams, J.A. (2001) *J. Biol. Chem. 17*, 14204-14211.

32. Rozovsky, S., and McDermott, A.E. (2001) *J. Mol. Biol. 310*, 259-270.

33. Shi, W., Li, C.M., Tyler, P.C., Furneaux, R.H., Grubmeyer, C., Shramm, V.L., and Almo, S.C. (1999) *Nat. Struct. Biol. 6*, 588-593.

34. Beach, H., Cole, R., Gill, M.L., and Loria, J.P. (2006) *J. Am. Chem. Soc. 127*, 9167-9176.

35. Lakowicz, J.R., Laczko, G., and Gryczynski, I. (1987) *Biochemistry 26*, 82-90.

36. Boyd, A.E., Dunlop, C.S., Wong, L., Radi, Z., Taylor, P., and Johnson, D.A. (2004) *J. Biol. Chem. 279*, 26612-26618.

37. Desamero, R., Rozovsky, S., Zhadin, N., McDermott, A., and Callender, R. (2003) *Biochemistry 42*, 2941-2951.

38. Eaazhisai, K., Balram, H., Balram, P., and Murthy, M.R.N. (2004) *J. Mol. Biol. 343*, 671-684.

39. Pattanaik, P., Ravindra, G., Sengupta, C., Maithal, K., Balaram, P., and Balaram, H. (2003) *Eur. J. Biochem. 270*, 745-756.

40. Eisenmesser, E.Z., Bosco, D.A., Akke, M., and Kern, D. (2002) *Science 295*, 1520-1524.

41. Codreanu, S.G., Ladner, J.E., Xiao, G., Stourman, N.V., Hachey, D.L., Gilliland, G.L., and Armstrong, R.N. (2002) *Biochemistry 41*, 15161-15172.

42. Gottschall, D.W., Dietrich, R.F., and Benkovic, S.J. (1982) *J. Biol. Chem. 257*, 845-849.

43. Haavik, J., Le Bourdelles, B., Martinez, A., Flatmark, T., and Mallet, J. (1991) *Eur. J. Biochem. 19*, 371-378.

44. Fitzpatrick, P.F. (1989) *Biochem. Biophys. Res. Commun. 161*, 211-215.

45. Balasubramanian, S., Carr, R.T., Bender, C.J., Peisach, J., and Benkovic, S.J. (1994) *Biochemistry 33*, 8532-8537.

46. Ramsey, A.J., Daubner, S.C., Ehrlich, J.I., and Fitzpatrick, P.F. (1995) *Prot. Sci. 4*, 2082-2086.

47. Fitzpatrick, P.F., Ralph, E.C., Ellis, H.R., Willmon, O.J., and Daubner, S.C. (2003) *Biochemistry 42*, 2081-2088.

48. Ellis, H.R., McCusker, K.P., and Fitzpatrick, P.F. (2002) *Arch. Biochem. Biophys. 408*, 305-307.

49. Bassan, A., Blomberg, M.R.A., and Siegbahn, P.E.M. (2003) *Chem. Eur. J. 9*, 106-115.

50. Ellis, H.R., Daubner, S.C., McCulloch, R.I., and Fitzpatrick, P.F. (1999) *Biochemistry 38*, 10909-10914.

51. Daubner, S.C., and Fitzpatrick, P.F. (1999) *Biochemistry 38*, 4448-4454.

52. Fitzpatrick, P.F. (1991) *Biochemistry 30*, 3658-3662.

53. Fitzpatrick, P.F. (2003) *Biochemistry 42*, 14083-14091.

54. Massey, V. (1994) *J. Biol. Chem. 269*, 22459-22462.

55. Francisco, W.A., Tian, G., Fitzpatrick, P.F., and Klinman, J.P. (1998) *J. Am. Chem. Soc. 120*, 4057-4062.

56. Hillas, P.J., and Fitzpatrick, P.F. (1996) *Biochemistry 35*, 6969-6975.

57. Moran, G.R., Derecskei-Kovacs, A., Hillas, P.J., and Fitzpatrick, P.F. (2000) *J. Am. Chem. Soc. 122*, 4535-4541.

58. Dix, T.A., Bollag, G., Domanico, P.L., and Benkovic, S.J. (1985) *Biochemistry 24*, 2955-2958.

59. Ellis, H.R., Daubner, S.C., and Fitzpatrick, P.F. (2000) *Biochemistry 39*, 4174-4181.

60. Price, J.C., Barr, E.W., Tirupati, B., Bollinger, J.M., and Krebs, C. (2003) *Biochemistry 42*, 7497-7508.

61. Siegmund, H.-U., and Kaufman, S. (1991) *J. Biol. Chem. 266*, 2903-2910.

62. Moran, G.R., Phillips, R.S., and Fitzpatrick, P.F. (1999) *Biochemistry 38*, 16283-16289.

63. Bailey, S.W., Rebrin, I., Boerth, S.R., and Ayling, J.E. (1995) *J. Am. Chem. Soc. 117*, 10203-10211.

64. Kappock, T.J., and Caradonna, J.P. (1996) *Chem. Rev. 96*, 2659-2756.

65. Zigmond, R.E., Schwarzschild, M.A., and Rittenhouse, A.R. ( 1989) *Ann. Rev. Neurosci. 12*, 415-461.

66. Kumer, S.C., and Vrana, K.E. (1996) *J. Neurochem. 67*, 443-462.

67. Cohen, P. (2000) *Trend. Biochem. Sci. 25*, 596-601.

68. Kansy, J.W., Daubner, S.C., Nishi, A., Sotogaku, N., Lloyd, D., Nguyen, C., Lu, L., Haycock, J.W., Hope, B.T., Fitzpatrick, P.F., and Bibb, J.A. (2004) *J. Neurochem. 91*, 374-384.

69. Vulliet, P.R., Hall, F.L., Mitchell, J.P., and Hardie, D.G. (1989) *J. Biol. Chem. 264*, 16292-16298.

70. Hall, F.L., Braun, R.K., Mihara, K., Fung, Y.-K.T., Berndt, N., Carbonaro-Hall, D.A., and Vulliet, P.R. (1991) *J. Biol. Chem. 266*, 17430-17440.

71. Toska, K., Kleppe, R., Armstron, C.G., Morrice, N.A., Cohen, P., and Haavik, J. (2002) *J. Neurochem. 83*, 775-783.

72. Campbell, D.G., Hardie, D.G., and Vulliet, P.R. (1986) *J. Biol. Chem. 261*, 10489-10492.

73. Sutherland, C., Alterio, J., Campbell, D.G., Le Bourdelles, B., Mallet, J., Haavik, J., and Cohen, P. (1993) *Eur. J. Biochem. 217*, 715-722.

74. Vulliet, P.R., Woodgett, J.R., Ferrari, S., and Hardie, D.G. (1985) *FEBS Letts. 182*, 335-339.

75. Roskoski, R.Jr., Vulliet, P.R., and Glass, D.B. (1987) *J. Neurochem. 48*, 840-845.

76. Daubner, S.C., Lauriano, C., Haycock, J.W., and Fitzpatrick, P.F. (1992) *J. Biol. Chem. 267*, 12639-12646.

77. McCulloch, R.I., and Fitzpatrick, P.F. (1999) *Arch. Biochem. Biophys. 367*, 143-145.

78. Royo, M., Fitzpatrick, P.F., and Daubner, S.C. (2005) *Arch. Biochem. Biophys. 423*, 252.

79. Ramsey, A.J., Hillas, P.J., and Fitzpatrick, P.F. (1996) *J. Biol. Chem. 271*, 24395-24400.

80. Frantom, P.A., Seravalli, J., Ragsdale, S.W., and Fitzpatrick, P.F. (2006) *Biochemistry 45*, 2372-2379.

81. Fitzpatrick, P.F. (1999) *Ann. Rev. Biochem. 68*, 355-381.

82. Daly, J., Levitt, M., Guroff, G., and Udenfriend, S. (1968) *Arch. Biochem. Biophys. 126*, 593-598.

83. Grenett, H.E., Ledley, F.D., Reed, L.L., and Woo, S.L.C. (1987) *Proc. Natl. Acad. Sci. USA 84*, 5530-5534.

84. Sura, G.R., Daubner, S.C., and Fitzpatrick, P.F. (2004) *J. Neurochem. 90,* 970-980.

85. Grima, B., Lamouroux, A., Boni, C., Julien, J.-F., Javoy-Agid, F., and Mallet, J. (1987) *Nature 326*, 707-711.

86. Lewis, D.A., Melchitzky, D.S., and Haycock, J.W. (1993) *Neuroscience 54*, 477-492.

87. Haycock, J.W. (1990) *J. Biol. Chem. 265*, 11682-11691.

88. Haycock, J.W., Ahn, N.G., Cobb, M.H., and Krebs, E.G. (1992) *Proc. Natl. Acad. Sci. USA 89*, 2365-2369.

89. Royo, M., Daubner, S.C., and Fitzpatrick, P.F. (2004) *Arch. Biochem. Biophys. 423*, 247-252.

90. Le Bourdellčs, B., Horellou, P., Le Caer, J.P., Denčfle, P., Latta, M., Haavik, J., Guibert, B., Mayaux, J.F., and Mallet, J. (1991) *J. Biol. Chem. 266*, 17124-17130.

91. Ramsey, A.J., and Fitzpatrick, P.F. (2000) *Biochemistry 39*, 773-778.

92. Haavik, J., Andersson, K.K., Petersson, L., and Flatmark, T. (1988) *Biochim. Biophys. Acta. 953*, 142-156.

93. Andersson, K.K., Vassort, C., Brennan, B.A., Que, L.Jr., Haavik, J., Flatmark, T., Gros, F., and Thibault, J. (1992) *Biochem. J. 284*, 687-695.

94. Kaneda, N., Kobayashi, K., Ichinose, H., Kishi, F., Nakazawa, A., Kurosawa, Y., Fujita, K., and Nagatsu, T. (1987) *Biochem. Biophys. Res. Commun. 147*, 971-975.

95. O'Malley, K.L., Anhalt, M.J., Martin, B.M., Kelsoe, J.R., Winfield, S.L., and Ginns, E.I. (1987) *Biochemistry 26*, 6910-6914.

96. Boularand, S. , Darmon, M.C., and Mallet, J. (1995) *J. Biol. Chem. 270*, 3748-3756.

97. Alterio, J., Ravassard, P., Haavik, J., Le Caer, J., Biguet, N., Waksman, G., and Mallet, J. (1998) *J. Biol. Chem. 273* , 10196-10201.

98. Flockhart, D.A., and Corbin, J.D. (1984) in *Brain Receptor Methodologies, Part*

*A* (Maranos, P.J., Campbell, I.C., & Cohen, R.M., Eds.) pp 209-215, Academic Press, New York.

99. McCulloch, R.I., Daubner, S.C., and Fitzpatrick, P.F. (2001) *Biochemistry 40*, 7273-7278.

100. Michaud-Soret, I., Andersson, K.K., Que, L.Jr., and Haavik, J. (1995) *Biochemistry 34*, 5504-5510.

101. Erlandsen, H., Flatmark, T., Stevens, R.C., and Hough, E. (1998) *Biochemistry 37*, 15638-15646.

102. Carlsson, A., Davis, J.N., Kehr, W., Lindqvist, M., and Atack, C.V. (1972) *Naunyn. Schmiedeberg's Arch. Pharmacol. 275*, 153-168.

103. Kehr, W., Carlsson, A., and Lindqvist, M. *Naunyn. Schmiedeberg's Arch. Pharmacol 274*, 273-280.

104. Wagner, J., Palfreyman, M., and Zraika, M. (1979) *J. Chromatogr. 164*, 41-54.

105. Buu, N.T., Duhaime, J., and Kuchel, O. (1985) *J. Neurochem. 44*, 787-792.

106. DeRobertis, E. (1967) *Science 156*, 907-914.

107. Serck-Hanssen, G., and Helle, K.B. (1972) *Biochim. Biophys. Acta. 273*, 199-207.

108. Kirshner, N. (1974) *Life Sci. 14*, 1153-1167.

109. Moad, G., Luthy, C.L., Benkovic, P.A., and Benkovic, S.J. (1979) *J. Am. Chem. Soc. 101*, 6068-6076.

110. Shiman, R., Jones, S.H., and Gray, D.W. (1990) *J. Biol. Chem. 265*, 11633-11642.

111. Perrin, F. (1926) *J. Phys. Radium V 7*, 390-398.

112. Weber, G. (1952) *Biochem. J. 51*, 145-155.

113. Spencer, R.D., and Weber, G. (1969) *Ann. N. Y. Acad. Sci. 158*, 361-376.

114. Weber, G. (1977) *J. Phys. Chem. 66*, 4081-4091.

115. Mantulin, W.W., and Weber, G. (1977) *J. Chem. Phys. 66*, 4092-4099.

116. Lipari, G., and Szabo, A. (1980) *Biophys. J. 30*, 489-506.

117. Johnson, J.L., and Reinhart, G.D. (1994) *Biochemistry 33*, 2644-2650.

118. Fitzpatrick, P.F. (1988) *J. Biol. Chem. 263*, 16058-16062.

119. Daubner, S.C., McGinnis, J.T., Gardner, M., Kroboth, S.L., Morris, A.R., and Fitzpatrick, P.F. (2006) *J. Mol. Biol.* (Under review)

120. Hvidt, A., and Linderstrom-Lang, K. (1954) *Biochim. Biophys. Acta 14*, 574-575.

121. Rosa, J.J., and Richards, F.M. (1979) *J. Mol. Biol 3*, 399-416.

122. Engen, J.R., and Smith, D.L. (2000) in *Methods in Molecular Biology, Volume 146, Protein and Peptide Analysis: New Mass Spectrometric Applications* (Anonymous) pp 95-112, Humana Press, Inc., Totowa, NJ.

123. Zhang, Z., and Marshall, A.G. (1998) *J. Am. Soc. Mass. Spetrom 9*, 225-233.

124. Zhang, Z., and Smith, D.L. (1993) *Protein Science 2*, 522-531.

125. Molday, R.S., Englander, S.W., and Kallen, R.G. (1972) *Biochemistry 11*, 150-158.

126. Smith, D.L., Deng, Y., and Zhang, Z. (1997) *J. Mass. Spectrom. 32*, 135-146.

127. Wasinger, E.C., Davis, M.I., Pau, M.Y.M., Orville, A.M., Zaleski, J.M., Hedman, B., Lipscomb, J.D., Hodgson, K.O., and Solomon, E.I. (2003) *Inorg. Chem. 42*, 365-376.

# VITA

GIRI RAJU SURA

**MAILING ADDRESS**
Department of Biochemistry and Biophysics
Texas A&M University, College Station, TX 77843-2128
Phone-(979)-845-6832

## EDUCATION

- Ph.D., Biochemistry, Texas A&M University, College Station, TX. May, 2006
- M.S., Biotechnology, Punjabi University, Patiala, Punjab-India, April, 2000
- B.S., Botany, Zoology and Chemistry, Osmania University, Hyderabad, Andhra Pradesh-India, April, 1998
- B.M.S, Medical Sciences, University of Health Sciences, Hyderabad, Andhra Pradesh-India, August, 1995

## AWARDS

- Second in Merit in M.S., Biotechnology
- CSIR fellowship in 2000

## MAJOR PUBLICATIONS

- Identification of Catalytic Residues in Tryptophan 2-Monooxygenase, a Homologue of L-Amino Acid Oxidase, Sobrado, P., Sura, G. R., and Fitzpatrick, P. F. (2002) *Flavins and Flavoproteins 2,* 369-374.
- Effect of phosphorylation by protein kinase A on binding of catecholamines to the human tyrosine hydroxylase isoforms, Sura, G.R., Daubner, S.C., and Fitzpatrick, P.F. (2004) *J. Neurochem. 90,* 970-980.